THE EFFECTS OF POTASSIUM AND SODIUM CATIONS ON THE PHASE AND MORPHOLOGY OF BISMUTH IRON OXIDE CRYSTALS

A Thesis

Presented to the Faculty of the Graduate School

of Cornell University

In Partial Fulfillment of the Requirements for the Degree of

Master of Science

by

Jeremy Lucas Fredricks

December 2018

ABSTRACT

Bismuth iron oxide (BFO) crystals have potential for applications ranging from next-generation, magnetoelectricity-based electronics to photocatalysts for the breakdown of toxic chemicals. Hydrothermal synthesis (HTS) has been shown to be an attractive solution growth method for producing well-defined, phase-pure BFO crystals. Until now, research in this field has focused on understanding the relationships between external experimental parameters in HTS and resultant crystalline phases of BFO, neglecting the role of the solution chemistry in crystal phase determination. Two spectator cations, Na^+ and K^+, commonly used in HTS of BFOs were investigated for their potential roles in determining the phase outcome of the final products in relation to a recently discovered, time-dependent transformation of an intermediate phase that was found to strongly influence the final phase outcome. Synthesis of BFOs was performed using wet chemistry techniques and reaction in a high-pressure, low-temperature environment. Characterization was performed using powder X-ray diffraction, scanning electron microscopy, and energy-dispersive X-ray spectroscopy. Phase-pure $BiFeO_3$ was confirmed to form in the presence of K^+ only when the intermediate underwent transformation while phase-pure $Bi_2Fe_4O_9$ could be formed in the presence of Na^+ regardless of the status of the intermediate. A new synthetic method was developed to elucidate whether the cations affected the transformation of the intermediate, and whether this potential transformation was the cause of the phase control. It was found that the intermediate was not crystallographically affected by the cations and the presence of the cations themselves only during heat treatment determined the final phase of the product. Finally, a thought experiment was conducted

that suggests a stabilization role for spectator anions and a formation mechanism for $Bi_2Fe_4O_9$. The effects of cations on crystal morphology were inconclusive. The methods developed for these investigations and subsequent results lay the groundwork for a better understanding of the role of other ions in the HTS of BFOs.

BIOGRAPHICAL SKETCH

Jeremy Fredricks was born in Fort Campbell, Kentucky, USA in 1993. In his early years, his family moved to Tennessee and Japan until settling in Florida when he was 5. Since his first exposure to science in middle school, he has always wanted to become a scientist, wavering very little in his aspirations as he grew up. Up to his senior year in high school, he was interested in pursuing chemistry in college until he set his sights on materials science after reading about it in a magazine. He was accepted to Cornell University where he majored in Materials Science and Engineering.

As an undergraduate, he took nearly every elective offered in the department on the different classes of materials. His interest in biomimetics and bioinspiration led him to join the Estroff Group as a junior. Under the guidance of Professor Estroff and PhD mentor Abby Goldman, he studied the hydrothermal synthesis of bismuth iron oxides. He continued his undergraduate research for his Master's Degree program, focusing on the effects of spectator ions commonly used in these syntheses. After graduation, he intends to pursue a doctorate degree in materials science at University of Washington.

DEDICATION

To those who read this thesis. Thank you.

ACKNOWLEDGMENTS

My thanks go out to the faculty and my peers in the Materials Science and Engineering Department at Cornell University for teaching me everything I know about materials science. In particular, I would like to thank Professors Baker, Nucci, and van Dover, whose interactions with me inside and outside of class helped me grow as a scientist and person. I thank the Estroff group for showing me how awesome research could be (the good and the bad parts) and being friendly and helpful. In particular, I thank Joo Ho Kim and Reum Scott, whose devotion to the lab and research served as inspiration to me in my work and to continue pursuing research as a career option. My biggest thanks go out to Professor Estroff, my advisor whose patience and advice all these years has helped me more than words can express, and Abby Goldman, who brought me under her wing and gave me encouragement, taught me how to write, think, and do lab work. I couldn't have asked for a better mentor. Without them, none of this would have been possible.

TABLE OF CONTENTS

Chapter 1.

Introduction and Background

Goal:

The main goal of this thesis is to grow crystals of different phases of bismuth iron oxides from an aqueous solution that contains dissolved salts of precursor bismuth and iron compounds, and to understand the crystallization pathway(s) leading to different bismuth iron oxide phases. To do this, we must understand (1.1) what factors affect the growth of these crystals from solution, (1.2) what these different phases are, (1.3) and what specific techniques we are using to grow these crystals in solution. Specifically, Chapter 1 will cover the basics required to understand why potassium and sodium cations may have an effect on the phase and morphology outcomes of crystals of bismuth iron oxide.

1.1 Crystallization Pathways

In general, crystallization is separated into an initial crystal nucleation stage and a subsequent crystal growth stage. For solutions that are capable of forming crystals, crystals can be synthesized solventless or with solvent. In the solventless case, all of the material in the solution, often called a melt, eventually crystallizes under a given set of conditions. With solvent, the solute nucleates out to form another phase of matter separate from the uncrystallized solvent. The following sections will be in the context of nucleation and growth in aqueous solvents.

1.1.1 Crystal nucleation in aqueous solutions

Dissolution is the process by which a compound is broken up into its constituent molecules or ions and solvated by solvent molecules. In water, the dissolution process usually involves a coordination of water molecules around the dissolved species to minimize a thermodynamic quantity called Gibbs free energy, *G*. *G* is defined as follows:

$$G(p,T) = H(p) - TS \quad (1)$$

where *p* is pressure of the system, *T* is the average temperature in the system, *H* is the enthalpy, and *S* is the entropy of the system. *G* is a measure of how much energy is available to do (non-pV) work in a given thermodynamic process. However, the value of *G* itself is usually not of much importance. In thermodynamically-controlled processes, such as many phase changes and chemical reactions, the *G* values for the individual components of the process are added together, giving significance to the change in Gibbs free energy, ΔG, as an indicator for whether the process will occur and to what extent. By convention, a theoretical process calculated in this manner will occur when the value of ΔG is negative, which is maximized when the entropy of the system increases ($\Delta S > 0$) and heat is released ($\Delta H < 0$).

Solvating water bonds constantly break and reform due to thermal fluctuations. The breaking and reforming of bonds allows the opportunity for dissolved species to randomly come into contact with other species in solution. When species come into contact with each other, they may temporarily, weakly bond due to electrostatic interactions. When several species are bonded together in such a manner within a short

period of time, a special type of cluster called a nucleus is formed, or nucleated. The nucleus becomes the precursor to crystal formation.

In classical nucleation theory, it is assumed that a nucleus takes on a roughly spherical shape as material is added to it until it becomes stable enough to become a crystal. Spheres are mathematically the most compact three-dimensional shape, meaning their surface area to volume ratio decrease faster with increasing volume than any other shape. A given amount of clustered material will maximize volume in nuclei. Maximization of volume is important because there are energetic costs associated with building a nucleus. Nucleation is a competition between the decrease in energy due to species leaving the solvent to become a part of the nucleus and the increase in energy due to formation and restructuring of the nucleus-solvent interface that occurs with every addition to the nucleus. In math terms (stated without proof):

$$\Delta G_N(r) = \frac{4}{3}\pi r^3 \Delta G_V + 4\pi r^2 \gamma \quad (2)$$

where ΔG_V is the change in volume free energy, r is the radius of the nucleus (assuming sphericity), and γ is the interfacial surface energy. By convention, in a situation where nuclei form spontaneously, ΔG_V is negative while γ is positive. ΔG_N is positive up to a critical radius after which it is energetically more favorable to keep increasing the size of the nucleus rather than dissolving it back into the solution. The reason for the increase in energy followed by a decrease is because of the aforementioned surface area to volume ratio. At small radii, the surface area to volume ratio is relatively large and the increase in energy due to creating a new interface outweighs the decrease that comes with adding to the volume. Past the critical radius, further additions of material yield greater decreases in energy, favoring continual growth. Thus, when nuclei form, they

will either increase in size enough to continue growing or will fail to reach critical size and will dissolve back into the solution.

Supersaturation

When a salt is put into solution, the salt may dissolve, as discussed above. Some salts have a limited solubility in aqueous solutions. At a given temperature, if more salt is added into solution than can be dissolved (i.e. if the solubility limit is surpassed), the solution becomes supersaturated. The degree of supersaturation is a driving force for crystallization. Supersaturation is defined mathematically as:

$$\sigma = (\mu_{ss} - \mu_{eq})/kT = ln\left(\frac{a_{ss}}{a_{eq}}\right) \quad (3)$$

where σ is the supersaturation, μ is chemical potential, k is Boltzmann's constant, T is temperature, ln is natural log, and a is chemical activity. Supersaturation affects both kinetic and thermodynamic aspects of crystal nucleation.

Thermodynamically, the higher the supersaturation, the smaller the cluster size requirement for a nucleus to continue growing spontaneously. A smaller critical cluster size corresponds to a lower free energy maximum to reach that size. Using the argument that *Davey & Garside*[1] uses and constructing a nucleus containing z amount of molecules, we can derive an equation for free energy with respect to the number of molecules in the nucleus and the supersaturation:

$$\Delta G(z) = -zkT\sigma + \beta\gamma z^{2/3} \quad (4)$$

where z is the number of molecules, β is a shape factor (and in fact, this derivation would work with other compact shapes), and γ is interfacial tension. We can then find how the critical size depends on the supersaturation:

$$z \propto \frac{1}{\sigma^3} \quad (5)$$

Alternatively

$$\mathrm{r} \propto \frac{1}{\sigma} \quad (6)$$

because *z* is proportional to the volume while *r* is proportional to the cube root of volume. Finally, it is possible to find how the free energy maximum changes with supersaturation:

$$\Delta G_{crit} \propto \frac{1}{\sigma^2} \quad (7)$$

Thus, a larger value of supersaturation allows for spontaneous crystal growth starting from smaller nucleus sizes.

Activity

Supersaturation relies on the concentration of species being above an equilibrium amount in order for crystallization to begin. However, concentration in real solutions is usually not as straightforward as knowing how much solute was put into solution for a given amount of solvent. Especially in the case of ionic species, electrical screening may reduce the effective concentration of species available to form crystals in the solution. Activity is the term used to denote the effective concentration in non-ideal solutions. Relatedly, the activity coefficient is a measure of how much the effective concentration deviates from the concentration that is calculated to be in the solution. Activity, *a*, is defined as:

$$a_i = \gamma_i \frac{c_i}{c^0} \quad (8)$$

where *i* refers to a specific species being measured, γ is the activity coefficient, and *c* is the concentration of the species, and c^0 is the standard state concentration, included to make activity dimensionless.

A useful example of the corrections that need to be taken into account in an ionic solution to measure the mean ionic activity (because activity of single ions cannot be experimentally measured) is that of the Debye-Hückel equation:

$$\log_{10}(\gamma_i) = -\frac{Az_i^2\sqrt{I}}{1+Br\sqrt{I}} \tag{9}$$

where *A* and *B* are temperature-dependent constants, z_i is the value of the charge on the ion, *r* is the distance of closest approach of ions (in extensions to the equations – the effective diameter or hydrated radius of the ion), and *I* is the ionic strength of the solution, defined as:

$$I = \frac{1}{2}\sum_{j=1}^{n} b_j z_j^2 \tag{10}$$

where b_j is the concentration (usually molarity or molality) of a particular ion species and z_j is the charge on an individual ion. The use of *I* takes into account the charges of all ionic solutes in aqueous solution, regardless of whether they take part in reactions. Thus, even non-reacting spectator ions have an influence on the activity of species that do react.

The biggest flaw with the Debye-Hückel equation is that it ceases to be accurate past small concentrations due to its simplicity. More accurate extensions based on it take into account a variety of factors such as the interactions between oppositely-charged ion pairs and higher order ion interactions[2,3] or solvent-solute ion interactions[4]. It is apparent from the accuracy of these models that ions in solution, especially at higher

concentrations, affect the activity of reactive species, potentially leading to the formation of unexpected intermediates or products.

Role of Spectator Ions in Non-Ideality of Solutions

Spectator ions are ions that do not directly take part in chemical reactions but are present in the reaction system, usually to maintain charge neutrality.[5] They may be coupled to species that react or may be introduced by the dissociation of unreactive salts. The following chemical reaction is an example of a reaction involving spectator ions:

$$AB(aq) + CD(aq) \rightleftharpoons A(aq) + D(aq) + BC(s, g)$$

BC is the product, either gaseous or solid, of this reaction. A and D are spectator ions, retaining their aqueous identities with no change through the course of the reaction of their counter-ions. The extent to which BC forms is dictated by the magnitude of the reaction's negative free energy change. Crystal formation of BC occurs if BC is solid and the reaction equilibrium shifts so far to the right that its equilibrium concentration is above the solubility threshold, forcing nucleation to restore equilibrium. The solubility of a crystal at equilibrium is related to the free energy by the relation:

$$\Delta G^0 = -RTlnK_{sp} \tag{11}$$

where, given the equilibrium reaction for the dissolution of a compound $\mathrm{M}_x\mathrm{N}_y(s) \rightleftharpoons XM^{y+}(aq) + YN^{x-}(aq)$,

$$K_{sp} = (a_{M^{y+}})^X (a_{N^{x-}})^Y \tag{12}$$

where *a* is the activity of a species. In this case, the higher the ΔG^0 value, the lower the solubility and the more easily a crystal will form, or not dissolve, given a supersaturated solution. A large, positive ΔG value corresponds to only a small amount of solvated

solute in solution. Interactions with the solvent are minimized when a crystal is large because the relative surface area to solvate is smaller than that of smaller, individual species.

The formation of crystals, then, is related to the activities of solutes which is dependent on the ionic strength of the solution. It follows that crystal formation may be influenced not just by the amount of reactant in solution (Equation (8)), but also by increased solution ionic strength by addition of charged species (Equation (9)). Adding acid or base would accomplish increasing ionic strength at the cost of potential side reactions or unintended complexes forming. Adding spectator ions increases ionic strength without contributing directly to side reactions. Careful manipulation of ionic strength could increase the activity coefficient, requiring a lower concentration of a species for the same value of activity. Since the activity of species dictates the equilibrium, the equilibrium could be shifted to form more or less product just by varying ionic strength and changing the type of spectator ion in solution (because interactions between ions are dependent on the size and charge of ions). Applying this thinking to multistep syntheses, controlling when spectator ions are put into solution may be a viable way of influencing the formation of intermediate species that are directly involved in the formation of the final products.

1.1.2 Crystal growth and morphology

Once a nucleus is stable enough to continue growing spontaneously, the crystal nucleation stage shifts to the crystal growth stage. As long as a solution is supersaturated, growth will occur. In an effort to keep reducing energy, the growth of faces on the

nucleus occurs. At this point, the nucleus is stable and material is added onto the nucleus at different speeds depending on the faces that are being constructed - a mix of quickly and slowly growing faces will appear. More generally, these speed differences are due to different planes in the crystal having different stabilities. Stabilities of planes are determined by the types of species that make up the crystal, the symmetry of the crystal, and the surrounding solution environment. A consequence of this growth difference is that the apparent faces, or expressed facets, in an ideal crystal are determined by the slowest growing planes. The fastest planes are bounded on every side by slower planes. As the fast planes grow, they are pinched down on all sides by the slowly growing planes until the slow planes meet at a point and crystal faces formed by fast, unstable planes disappear.

The surface of the crystal is defined by faces, edges, and corners, as with any shape of finite size. Faces are the most stable because any species in the face will be stabilized by the species surrounding it, on every side except the surface. Accordingly, edges and then corners are progressively higher in energy because there are fewer neighbors to stabilize them. Less dense planes grow faster than denser, stable planes in an effort to satisfy their dangling bonds and remove excess energy.

Relationship of nucleation to growth

Nucleation exists as a way to decrease the degree of supersaturation in a solution. When the supersaturation decreases, the energy required to form spontaneously growing nuclei increases. Because it requires less energy to keep adding to a preexisting nucleus, already-formed nuclei continue to grow at the expense of creating new nuclei. The

higher the initial degree of supersaturation is, the greater the number of nuclei in solution. After the nucleation period, the material left in solution is only used to grow the nuclei. If there are many nuclei, each nucleus receives less material to grow with than if there were fewer nuclei. Thus, there is an inverse relationship between the number of crystals and their sizes. One way to manipulate crystal growth, then, would be to limit the degree of supersaturation. A time-dependent amount of nuclei could be allowed to form, and then the amount of material that is left would be used to grow the present nuclei, allowing a more uniform distribution of crystal sizes.

One consequence of the relationship between crystal sizes and number is that crystals facets may not be well-defined at a given moment in time since the time required to sequester material to grow planes increases per nucleus. As a result, syntheses with short reaction times may result in formation of ill-defined crystals. However, facet definition does not necessarily reflect the stability of the crystals themselves, as the cores of ill-defined crystals may be regular, depending on the formation mechanism. Thus, possible explanations for why a crystal does not have a characteristic morphology include incomplete growth, non-classical growth mechanism (explained in the next section), or crystalline defects from impurity incorporation.

Crystal formation mechanisms

The discussion up to now has assumed a classical model of crystal nucleation and growth. In this model, crystals are nucleated by the attachment of simple particles or compounds to each other. Crystals grow by the individual adsorption and incorporation of these same units onto the nucleus.[6] A few consequences of this theory are that crystals

are unstable until large enough and that growing nuclei's internal structure is the same as their resultant crystals'.[7] However, recent research has shown that these assumptions are not accurate for all materials. A thorough discussion is outside of the scope of this thesis, but many good reviews exist discussing non-classical crystallization in depth.[8,9]

A non-classical crystallization pathway relevant for this discussion is that of two-step crystallization via a metastable phase.[8] Precursors react to form a metastable intermediate phase that eventually transforms into a desired final phase. One reason this mechanism occurs is because the intermediate phase may have a lower energy barrier to form compared to a more stable phase. The system benefits from forming this phase because its formation results in a lower overall free energy while transforming into a more stable phase may be infeasible in present conditions. A transformation from this intermediate into the final phase is then possible under a change in conditions such as pH or solution temperature. The transformation mechanism is not limited by this pathway and there are two relevant mechanisms for this discussion: solid-state transformation and dissolution-reprecipitation.

A solid-state transformation from the intermediate to a final phase occurs by local structural reorganizations inside of the intermediate, induced by changing conditions.[10] These conditions could be thermally-induced or by the addition of precursors which react with only the intermediate. Changing conditions cause a new phase to be more thermodynamically favorable than the intermediate phase. Local transformations occur throughout the intermediate, resulting in the nucleation of crystals of the more stable phase. If the new conditions persist, eventually all of the intermediate transforms into the new phase.

Intermediates can also transform to the final phase via dissolution-reprecipitation (sometimes called dissolution-recrystallization[8,11–14]). Dissolution-reprecipitation is a mechanism where the intermediate phase is dissolved back into the solution and then recrystallizes into another phase.[15] Similar to the solid-state transformation, the energy landscape changes when conditions are altered, causing the intermediate to become unstable or more soluble under the new conditions and to dissociate into its precursor units. The precursor units then directly transform into the final phase which becomes attainable under the new conditions. In this case, though transformation occurred in two steps, the new phase effectively forms by classical nucleation.

Dissolution-reprecipitation does not require the kinetics of the dissolution to be fast – local dissolution can give rise to the conditions and material necessary to precipitate the new phase at the point of dissolution, allowing for the possibility for both phases to coexist at short time scales.[16] For this reason, differentiating solid-state transformation from dissolution-reprecipitation is not trivial and may require the use of more sophisticated *in-situ* techniques to resolve the mechanism. Recent advances in TEM techniques (e.g. cryogenic, liquid-phase) are promising in being able to more easily differentiate such reaction mechanisms.[17,18]

Another consequence of non-classical crystallization is its potential effect on crystal morphology. Instead of individual species adding to a nucleus, research suggests that species can first form metastable clusters that combine with each other to make larger, more stable structures made of these clusters.[8] Crystalline clusters with characteristic shapes and bonding orientations can combine as seamless continuations onto a larger crystal, allowing the formation of atypical, single-crystalline shapes. This process is

known as crystallization by oriented attachment. More generally, crystallization by particle attachment allows for the possibility of asymmetric or chemically uneven crystals with properties that deviate from that of classically nucleated crystals.

Properties and morphology

The base properties of a material are dictated by its crystal structure. However, crystal size and morphology can influence the properties. Small sizes make the discrete nature of particles in a crystal more prevalent, making it possible to obtain properties not seen in the bulk crystal. An example of a size effect is bandgap tuning, which is used to control the colors of quantum dots.[19] Crystals with spatially variant properties can be made smaller to minimize the negative effects of the variance. For example, making ferromagnetic crystals small allows the formation of single magnetic domains, maximizing remanent magnetization for a single crystal.[20] Anisotropic crystals may be shaped to emphasize their crystallographic easy axes to maximize their electromagnetic effects.[20–22] Additionally, some properties are not predictable based solely on a structure perspective. For example, the catalytic properties of a material often differ between the planes of a crystal.[23] Different crystal morphologies can be crafted to maximize or minimize the exposure of specific planes to improve catalytic ability.

1.2 Family of Bismuth Iron Oxides: Structure, Properties, and Applications

Bismuth iron oxides (BFO) are of the chemical form $Bi_xFe_yO_z$, where x, y, and z are numbers indicating the stoichiometry of atoms in a unit cell. Different ratios of these numbers give rise to different phases of BFO with varying properties. The following is

an introduction to three such BFO compounds that will be encountered in the remainder of this thesis.

1.2.1 $BiFeO_3$

Structure

The compound commonly referred to as "bismuth ferrite" in the literature has the chemical formula $BiFeO_3$. $BiFeO_3$ has a rhombohedral crystal structure at room temperature with space group R3c.[24] Although rhombohedral crystal systems are usually described with hexagonal coordinates, $BiFeO_3$ has commonly been described with a pseudocubic crystal structure such that the c-axis in the hexagonal system is parallel to the [111] direction in the pseudocubic system (*Figure 1.1*). Common morphologies of bulk crystals include cylinders[25,26], cube-like[12,27–29], and octahedral[11,27,29,30].

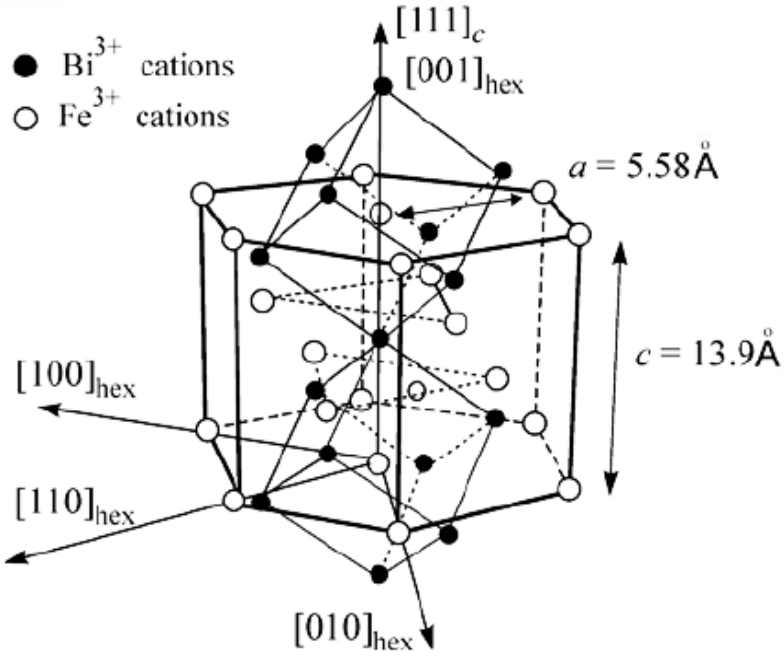

Figure 1.1: Crystal structure of $BiFeO_3$. The pseudocubic representation is overlayed on top of the hexagonal to emphasize the direction of spontaneous electrical polarization along $[111]_{pseudocubic}$. (Adapted from *Kadomtseva et al.*[24])

Properties

The pseudocubic representation is used to describe $BiFeO_3$'s properties more intuitively – it is ferroelectric due to polarization of $6s^2$ electrons on Bi^{3+} along the $[111]_{pseudocubic}$ axis and has antiferromagnetic order along planes of Fe^{3+} ions perpendicular to this axis.[24,31] $BiFeO_3$ exhibits the magnetoelectric effect, meaning the polarization can be controlled by a magnetic field and magnetization can be induced by an electric field, at room temperature.

Applications

There are currently no applications, but research into $BiFeO_3$ seeks to exploit its magnetoelectric properties. This magnetoelectric coupling allows for potential applications in next-generation devices such as spintronics, devices that manipulate the spins of the electrons to provide an extra degree of freedom for device control. An application of these devices include data storage devices whose data can be electrically-written and magnetically-read through spin-coupled interactions.[32]

1.2.2 $Bi_2Fe_4O_9$

Structure

$Bi_2Fe_4O_9$ is also referred to as a "mullite" material in the literature. It is an orthorhombic material with space group Pbam. The most common morphology for $Bi_2Fe_4O_9$ crystals via solution growth is rectangular sheets and cubes.[33–38]

Properties

Although paramagnetic at room temperature, it has a magnetic ordering temperature $T_N \approx 264$ K below which it is antiferromagnetic.[35,39–41] $Bi_2Fe_4O_9$ is a semiconductor material with a bandgap that has been shown to be easily tunable in the range of 1.9 to 2.3 eV, depending on the thickness of the sheets.[33,37]

Applications

Due to its semiconductor properties, it has potential to serve in applications where a semiconductor may typically be used. Other applications include its use as an ammonium oxidation catalyst to form NO gas, potentially replacing more costly catalysts.[41] Recent studies have shown that it works well as a photocatalyst for the breakdown of organic compounds such as methyl orange and rhodamine B.[33,35,42] Another study demonstrated its efficacy in removal of heavy metal ions in aqueous solutions for environmental remediation applications.[42]

1.2.3 $Bi_{25}FeO_{40}$

Structure

$Bi_{25}FeO_{40}$ is commonly also reported as $Bi_{25}FeO_{39}$ in the literature and also often referred to as a "sillenite" material.[43,44] It has cubic space group I23. It has been reported to have one Bi^{5+} ion per unit cell to balance the excess negative charge of the O^{2-} whereas all other Bi and Fe ions are in the 3+ oxidation state.[43]

Properties

Sillenite materials are often studied due to their common photonic properties (e.g. photo-refractive, photo-conductive, electro-optic, etc.). $Bi_{25}FeO_{40}$ has been shown to have very good mobility of photogenerated charges, marking its use as a photocatalyst.[44,45]

Applications

$Bi_{25}FeO_{40}$ has been used for the photocatalytic degradation of various organic toxins.[45,46]

1.2.4 Thermodynamic relationships between BFOs

Phapale et al. derived the standard Gibbs energy of formation as a function of temperature ($\Delta_f G^0(T)$) from experimental data and tabulated values for molar heat capacity, enthalpy of formation, and standard molar entropy.[47] Their results are summarized in Table 1.1. These results imply that BFOs are stable compounds formed from their respective oxide precursors, but $BiFeO_3$ is the least stable among these. This stability ranking poses a nontrivial problem for those seeking to preferably synthesize $BiFeO_3$ as the other compounds are more likely to form using traditional solid-state synthesis methods.

Table 1.1

Compound	$\Delta_f G^0(T)$ / kJ mol^{-1}	$\Delta_f G^0(298.15\ K)$ / kJ mol^{-1}	$\Delta_f G^0(473\ K)$ / kJ mol^{-1}
$BiFeO_3$	-773.3 + 0.269T	-693.1	-643.4
$Bi_2Fe_4O_9$	-2459.1 + 0.757T	-2233	-2101
$Bi_{25}FeO_{40}$	-7355.2 + 2.669T	-6559	-6093

Ostwald's Rule of Stages

Ostwald's Rule of Stages is an observation of the tendency of some materials to nucleate less-stable crystal structures first and then progressively transform into more stable crystal structures.[7] These crystal structures are polymorphs of each other – Encyclopedia Britannica defines polymorphism as "the ability of a [material of a] specific chemical composition to crystallize in more than one form".[48] A polymorphic

material would go from a supersaturated state to equilibrium in steps, from most soluble crystal structure to least.

Despite having similar ratios, $BiFeO_3$, $Bi_2Fe_4O_9$, and $Bi_{25}FeO_{40}$ are not polymorphs: their chemical compositions are distinct. However, mentioning Ostwald's Rule may be instructive for considering how these compounds nucleate under varying conditions from the same sets of starting salts or intermediates. The idea that a less stable intermediate can give way to a more stable final product will be useful for later discussion.

1.3 Hydrothermal synthesis

1.3.1 Background

Hydrothermal synthesis (HTS) is a geological synthesis method where water is the solvent and high pressures and temperatures are used to control the types of crystals formed. HTS can be recreated on a lab-scale by using a pressure-resistant, chemically-inert containment vessel as the reaction chamber (*Figure. 1.2*).[49] For condensed systems, such as aqueous solutions, increases in pressure may not cause substantial changes to solution chemistry. Instead, a closed environment allows reactions to occur at temperatures above the boiling point of the solvent without loss of material. For volatile or metastable reactants, hydrothermal synthesis offers a productive way to perform reactions at much lower temperatures than would be required in air without the support of species transport and solvent stabilization.[50]

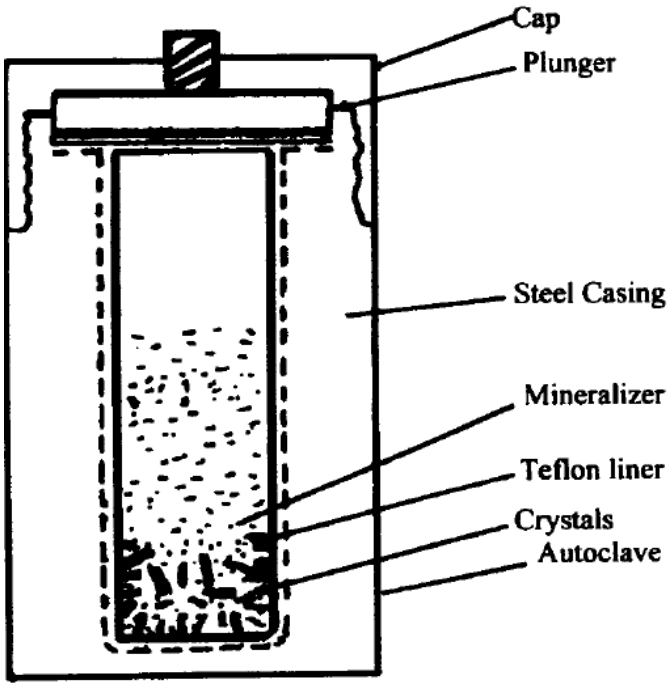

Figure 1.2: A classic hydrothermal reaction vessel. The main features are an unreactive inner chamber (Teflon liner) surrounded by a steel casing with a threaded lid. These safety features ensure reactions that require high pressures can be contained. (Adapted from *Byrappa et al.*[49])

The terms mineralizer and nutrient are often mentioned in the HTS literature. Mineralizers are additives that aid in the transport of insoluble or sparingly soluble solutes, called nutrients, to growing crystals. Mineralizers are thought to form soluble complexes with the nutrients. In HTS of BFOs, Bi^{3+} and Fe^{3+} are the nutrients that are thought to be complexed by OH^- base mineralizers.

1.3.2 Application to BFO growth

HTS has been used to synthesize BFOs since at least 2004, with reports of phase-pure and mixed-phase syntheses of $Bi_2Fe_4O_9$, $BiFeO_3$, and $Bi_{25}FeO_{40}$.[51] Since then, a variety of conditions and variables has been used and their results compared. Some commonly manipulated variables have included temperature[11,29,52–55], chemical additives/surfactants[14,53,56–65], and solution chemistry (esp. pH and reactant

ratios)[26,37,66–68]. Microwave HTS[13,57,69,70] has also been used as an alternative to traditional furnace heating. Temperature studies often include varying heating temperature, heating dwell time, and heating/cooling rate. Commonly added additives or surfactants include PVA, PVP, acetone, polyethylene glycol, and other organic substances. Solution chemistry manipulation includes varying concentration of OH^- used, varying relative amounts of metal ions[35,54,71], changing spectator ions on the base and reactants, and adding or removing spectator ions from the solution. However, using combinations of these variables is common, making it difficult to draw direct conclusions about the effects of individual parameters.

In 2006, *Chen et al.* and *Han et al.* investigated how reaction temperature, OH^- concentration and pH, and reaction time affected the final products.[52,72] They were the first groups to suggest a dissolution-reprecipitation mechanism of BFO crystal formation, which seems to be the common consensus in this field. Another mechanism of nucleation and growth that has been suggested is oriented attachment.[28,35] In both cases, a lack of *in-situ* reaction data prevent confirmation of the true mechanisms.

In 2007, *Wang et al.* published a paper providing evidence that the counter-ions on the OH^- base, Li^+, Na^+, and K^+, could influence phase control.[73] They hypothesized that these cations affected the solubilities of Bi^{3+} and Fe^{3+} ions. *Cai et al.* and *Lopes et al.* both reported the transformation of a crystalline $Bi_{25}FeO_{40}$-rich intermediate phase into $BiFeO_3$ with increasing heating time.[44,60] Both also detected an amorphous phase present along with the crystalline phases. *Lopes et al.* showed SEM images of $BiFeO_3$ crystals growing on top of or out from the intermediates. Despite how much time has elapsed since the publication of these papers, no mechanisms have been published that

explain how either cations or intermediates play a role in BFO formation. Further investigation of how these components contribute to formation of BFOs may lead to better understanding of the formation mechanisms of the BFO system.

1.4 Thesis objectives

Our most recent work built on what *Lopes et al.* and *Cai et al.* had discovered about the connection between the intermediates and final phases.[28] We confirmed that $Bi_{25}FeO_{40}$ was productive for the preferential formation of $BiFeO_3$ – when $Bi_{25}FeO_{40}$ was present in solution, the final product was phase-pure $BiFeO_3$. However, when $Bi_{25}FeO_{40}$ did not form but all other conditions were the same, a single phase of $Bi_2Fe_4O_9$ or a mixed phase of $BiFeO_3$ + $Bi_2Fe_4O_9$ resulted. Our work gave us a good foundation of conditions to use and their respective results in addition to the discovery of the potential importance of the presence of the $Bi_{25}FeO_{40}$ intermediate. We set out to try to confirm how changing the spectator counter-ion on the base, from K^+ to Na^+, would lead to changes in phase and morphology under otherwise same conditions. The results are detailed in Chapter 2.

1.5 References

(1) Davey, R.; Garside, J. Chapter 3: Nucleation. In *From Molecules to Crystallizers: An Introduction to Crystallization*; Oxford University Press, 2001; pp 15–16.

(2) Kim, H. T.; Frederick, W. J. Evaluation of Pitzer Ion Interaction Parameters of Aqueous Electrolytes at 25°C. 1. Single Salt Parameters. *J. Chem. Eng. Data* **1988**, *33* (2), 177–184.

(3) Kim, H. T.; Frederick, W. J. Evaluation of Pitzer Ion Interaction Parameters of Aqueous Mixed Electrolyte Solutions at 25 °C. 2. Ternary Mixing Parameters. *J. Chem. Eng. Data* **1988**, *33* (3), 278–283.

(4) Ge, X.; Wang, X.; Zhang, M.; Seetharaman, S. Correlation and Prediction of Activity and Osmotic Coefficients of Aqueous Electrolytes at 298.15 K by the Modified TCPC Model. *J. Chem. Eng. Data* **2007**, *52* (2), 538–547.

(5) Oxtoby, D. W.; Gillis, H. P.; Campion, A. Index/Glossary. In *Principles of Modern Chemistry, 6th Ed.*; 2008; p I.25.

(6) Ivanov, V. K.; Federov, P. P.; Baranchikov, A. Y.; Osiko, V. V. Oriented Attachment of Particles: 100 Years of Investigations of Non-Classical Crystal Growth. *Russ. Chem. Rev.* **2014**, *83* (12), 1204–1222.

(7) Schmelzer, J. W. P.; Abyzov, A. S. Chapter 9: How Do Crystals Nucleate and Grow: Ostwald's Rule of Stages and Beyond. In *Thermal Physics and Thermal Analysis: From Macro to Micro, Highlighting Thermodynamics, Kinetics and Nanomaterials*; Sestak, J., Hubik, P., Mares, J. J., Eds.; Springer International Publishing Switzerland, 2017; Vol. 11, pp 195–211.

(8) De Yoreo, J. J.; Gilbert, P. U. P. A.; Sommerdijk, N. A. J. M.; Penn, R. L.; Whitelam, S.; Joester, D.; Zhang, H.; Rimer, J. D.; Navrotsky, A.; Banfield, J. F.; et al. Crystallization by Particle Attachment in Synthetic, Biogenic, and Geologic Environments. *Science (80-.).* **2015**, *349* (6247), 6760 (1-9).

(9) De Yoreo, J. J. A Holistic View of Nucleation and Self-Assembly. *MRS Bull.* **2017**, *42* (7), 525–531.

(10) Carter, C. B.; Norton, M. G. Solid-State Phase Transformations and Reactions. In *Ceramic Materials: Science and Engineering*; Springer Science+Business Media, LLC., 2007; pp 445–449.

(11) Chen, X. Z.; Qiu, Z. C.; Zhou, J. P.; Zhu, G.; Bian, X. B.; Liu, P. Large-Scale Growth and Shape Evolution of Bismuth Ferrite Particles with a Hydrothermal Method. *Mater. Chem. Phys.* **2011**, *126* (3), 560–567.

(12) Zhou, J. P.; Yang, R. L.; Xiao, R. J.; Chen, X. M.; Deng, C. Y. Structure and Phase Transition of $BiFeO_3$ Cubic Micro-Particles Prepared by Hydrothermal Method. *Mater. Res. Bull.* **2012**, *47* (11), 3630–3636.

(13) Li, S.; Nechache, R.; Davalos, I. A. V.; Goupil, G.; Nikolova, L.; Nicklaus, M.; Laverdiere, J.; Ruediger, A.; Rosei, F. Ultrafast Microwave Hydrothermal Synthesis of $BiFeO_3$ Nanoplates. *J. Am. Ceram. Soc.* **2013**, *96* (10), 3155–3162.

(14) Chen, Z.; Jin, W. Low-Temperature Acetone-Assisted Hydrothermal Synthesis and Characterization of $BiFeO_3$ Powders. *J. Mater. Sci. Mater. Electron.* **2014**, *25* (9), 4039–4045.

(15) Modeshia, D. R.; Walton, R. I. Solvothermal Synthesis of Perovskites and Pyrochlores : Crystallisation of Functional Oxides under Mild Conditions. *Chem. Soc. Rev.* **2010**, *39*, 4303–4325.

(16) Rong, J.; Wang, F. Chapter 2: Formation Mechanisms for Mineral Replacement. In *Metasomatic Textures in Granites*; Springer Mineralogy; Science Press Ltd., 2016; pp 53–68.

(17) De Yoreo, J. J.; Sommerdijk, N. A. J. M. Investigating Materials Formation with Liquid-Phase and Cryogenic TEM. *Nat. Rev. Mater.* **2016**, *1* (8), 16035 (1-18).

(18) Walker, J. M.; Marzec, B.; Nudelman, F. Solid-State Transformation of Amorphous Calcium Carbonate to Aragonite Captured by CryoTEM. *Angew. Chemie - Int. Ed.* **2017**, *56* (39), 11740–11743.

(19) Wolf, E. L. 4.6.5 - Trapped Particles in Two and Three Dimensions: Quantum Dot. In *Nanophysics and Nanotechnology: An Introduction to Modern Concepts in Nanoscience*; Wiley-VCH Verlag GmbH & Co., 2004; pp 10–11, 62–63.

(20) Leslie-Pelecky, D. L.; Rieke, R. D. Magnetic Properties of Nanostructured Materials. *Chem. Mater.* **1996**, *8* (8), 1770–1783.

(21) Poole Jr., C. P.; Owens, F. J. 7.3 - Dynamics of Nanomagnets. In *Introduction to Nanotechnology*; John Wiley & Sons, Inc., 2003; pp 174–176.

(22) Buschow, K. H. J.; De Boer, F. R. 12.8 - Alnico Magnets. In *Physics of Magnetism and Magnetic Materials*; Kluwer Academic Publishers, 2004; pp 125–128.

(23) van Santen, R. A. 3.3 Elementary Kinetics. In *Modern Heterogeneous Catalysis: An Introduction*; Wiley-VCH Verlag GmbH & Co., 2017; pp 79–83.

(24) Kadomtseva, A. M.; Popov, Y. F.; Pyatakov, A. P.; Vorob'Ev, G. P.; Zvezdin, A. K.; Viehland, D. Phase Transitions in Multiferroic $BiFeO_3$ Crystals, Thin-Layers, and Ceramics: Enduring Potential for a Single Phase, Room-Temperature Magnetoelectric "Holy Grail." *Phase Transitions* **2006**, *79* (12), 1019–1042.

(25) Di, L. J.; Yang, H.; Xian, T.; Ma, J. Y.; Zhang, H. M.; Jiang, J. L.; Wei, Z. Q.; Feng, W. J. Growth of $BiFeO_3$ Microcylinders under a Hydrothermal Condition. *J. Nanomater.* **2015**, *2015* (3), 1–5.

(26) Zhou, M.; Li, W.; Du, Y.; Kong, D.; Wang, Z.; Meng, Y.; Sun, X.; Yan, T.; Kong, D.; You, J. Hydrothermal Synthesis of Bismuth Ferrite Fenton-like Catalysts and Their Properties. *J. Nanoparticle Res.* **2016**, *18* (11), 346 (1-15).

(27) Suzuki, K.; Tokudome, Y.; Tsuda, H.; Takahashi, M. Morphology Control of $BiFeO_3$ Aggregates via Hydrothermal Synthesis. *J. Appl. Crystallogr.* **2016**, *49* (1), 168–174.

(28) Goldman, A. R.; Fredricks, J. L.; Estroff, L. A. Exploring Reaction Pathways in the Hydrothermal Growth of Phase-Pure Bismuth Ferrites. *J. Cryst. Growth* **2017**, *468* (September 2016), 104–109.

(29) Xu, X.; Xu, Q.; Huang, Y.; Hu, X.; Huang, Y.; Wang, G.; Hu, X.; Zhuang, N. Control of Crystal Phase and Morphology in Hydrothermal Synthesis of $BiFeO_3$ Crystal. *J. Cryst. Growth* **2016**, *437*, 42–48.

(30) Hou, L.; Lu, Z. Y.; Dai, Y. C.; Zuo, K. H.; Xia, Y. F.; Ren, Z. M.; Wu, J.; Lu, X. G.; Zeng, Y. P.; Li, X. Self-Assembled Growth of $BiFeO_3$ Meso-Octahedral Particles Synthesized by a Facile Surfactant-Free Hydrothermal Method. *J. Cryst. Growth* **2016**, *434*, 42–46.

(31) Spaldin, N. A.; Cheong, S. W.; Ramesh, R. Multiferroics: Past, Present, and Future. *Phys. Today* **2010**, *63* (10), 38–43.

(32) Catalan, G.; Scott, J. F. Physics and Applications of Bismuth Ferrite. *Adv. Mater.* **2009**, *21* (24), 2463–2485.

(33) Ruan, Q.-J.; Zhang, W.-D. Tunable Morphology of $Bi_2Fe_4O_9$ Crystals for Photocatalytic Oxidation. *J. Phys. Chem. C* **2009**, *113* (10), 4168–4173.

(34) Du, Y.; Cheng, Z.; Dou, S.; Wang, X. Tunable Morphology and Magnetic Properties of $Bi_2Fe_4O_9$ Nanocrystal Synthesized by Hydrothermal Method. *J. Nanosci. Nanotechnol.* **2011**, *11* (3), 2691–2695.

(35) Zhang, X.; Lv, J.; Bourgeois, L.; Cui, J.; Wu, Y.; Wang, H.; Webley, P. A. Formation and Photocatalytic Properties of Bismuth Ferrite Submicrocrystals with Tunable Morphologies. *New J. Chem.* **2011**, *35* (4), 937–941.

(36) Cai, D.; Du, D.; Yu, S.; Cheng, J. Oriented Growth of $Bi_2Fe_4O_9$ Crystal and Its Photocatalytic Activity. *Procedia Eng.* **2012**, *27* (2011), 577–582.

(37) Tsai, C. J.; Yang, C. Y.; Liao, Y. C.; Chueh, Y. L. Hydrothermally Grown Bismuth Ferrites: Controllable Phases and Morphologies in a Mixed KOH/NaOH Mineralizer. *J. Mater. Chem.* **2012**, *22* (34), 17432–17436.

(38) Wu, T.; Liu, L.; Pi, M.; Zhang, D.; Chen, S. Enhanced Magnetic and Photocatalytic Properties of $Bi_2Fe_4O_9$ Semiconductor with Large Exposed (001) Surface. *Appl. Surf. Sci.* **2016**, *377*, 253–261.

(39) Han, J. T.; Huang, Y. H.; Jia, R. J.; Shan, G. C.; Guo, R. Q.; Huang, W. Synthesis and Magnetic Property of Submicron $Bi_2Fe_4O_9$. *J. Cryst. Growth* **2006**, *294* (2), 469–473.

(40) Zhang, X.; Bourgeois, L.; Yao, J.; Wang, H.; Webley, P. A. Tuning the Morphology of Bismuth Ferrite Nano- And Microcrystals: From Sheets to

Fibers. *Small* **2007**, *3* (9), 1523–1528.

(41) Park, T. J.; Papaefthymiou, G. C.; Moodenbaugh, A. R.; Mao, Y.; Wong, S. S. Synthesis and Characterization of Submicron Single-Crystalline $Bi_2Fe_4O_9$ Cubes. *J. Mater. Chem.* **2005**, *15* (21), 2099–2105.

(42) Kong, M.; Song, H.; Li, F.; Dai, D.; Gao, H. Facile Synthesis of $Bi_2Fe_4O_9$ Nanoplate and Its Application as a Novel Adsorbent for Cu(II) Removal. *J. Environ. Chem. Eng.* **2017**, *5* (1), 69–78.

(43) Köferstein, R.; Buttlar, T.; Ebbinghaus, S. G. Investigations on $Bi_{25}FeO_{40}$ Powders Synthesized by Hydrothermal and Combustion-like Processes. *J. Solid State Chem.* **2014**, *217* (September 2014), 50–56.

(44) Lopes, A. M. L.; Araújo, J. P.; Ferdov, S. Room Temperature Synthesis of $Bi_{25}FeO_{39}$ and Hydrothermal Kinetic Relations between Sillenite- and Distorted Perovskite-Type Bismuth Ferrites. *Dalt. Trans.* **2014**, *43* (48), 18010–18016.

(45) Zhang, L.; Zhang, X.; Zou, Y.; Xu, Y.-H.; Pan, C.-L.; Hu, J.-S.; Hou, C.-M. Hydrothermal Synthesis, Influencing Factors and Excellent Photocatalytic Performance of Novel Nanoparticle-Assembled $Bi_{25}FeO_{40}$ Tetrahedrons. *CrystEngComm* **2015**, *17* (34), 6527–6537.

(46) Köferstein, R.; Buttlar, T.; Ebbinghaus, S. G. Investigations on $Bi_{25}FeO_{40}$ Powders Synthesized by Hydrothermal and Combustion-like Processes. *J. Solid State Chem.* **2014**, *217*, 50–56.

(47) Phapale, S.; Mishra, R.; Das, D. Standard Enthalpy of Formation and Heat Capacity of Compounds in the Pseudo-Binary Bi_2O_3-Fe_2O_3 System. *J. Nucl. Mater.* **2008**, *373* (1–3), 137–141.

(48) Klein, C. Mineral: Chemical Compound - Polymorphism. *Encyclopædia Britannica*; Encyclopædia Britannica, Inc., 2018.

(49) Byrappa, K.; Lokanatha Rai, K. M.; Yoshimura, M. Hydrothermal Preparation of TiO_2 and Photocatalytic Degradation of Hexachlorocyclohexane and Dichlorodiphenyltrichloromethane. *Environ. Technol.* **2000**, *21* (10), 1085–1090.

(50) Byrappa, K. Chapter 18: Hydrothermal Growth of Polyscale Crystals. In *Springer Handbook of Crystal Growth*; 2010; pp 599–653.

(51) Xiong, Y.; Wu, M.; Peng, Z.; Jiang, N.; Chen, Q. Hydrothermal Synthesis and Characterization of $Bi_2Fe_4O_9$ Nanoparticles. *Chem. Lett.* **2004**, *33* (5), 502–503.

(52) Chen, C.; Cheng, J.; Yu, S.; Che, L.; Meng, Z. Hydrothermal Synthesis of Perovskite Bismuth Ferrite Crystallites. *J. Cryst. Growth* **2006**, *291* (1), 135–139.

(53) Qiu, Z. C.; Zhou, J. P.; Zhu, G.; Chen, X. Z.; Chen, X. M.; Liu, P. Hydrothermal Synthesis of Perovskite Bismuth Ferrite Crystallites with the Help of NH_4Cl. *J. Nanoparticle Res.* **2012**, *12* (8), 6552–6557.

(54) Zhang, H.; Kajiyoshi, K. Hydrothermal Synthesis and Size-Dependent Properties of Multiferroic Bismuth Ferrite Crystallites. *J. Am. Ceram. Soc.* **2010**, *93* (11), 3842–3849.

(55) Yan, D.; Sun, C.; Jian, J.; Sun, Y.; Wu, R.; Li, J. Structure and Phase Transition of $BiFeO_3$ Particles Prepared by Hydrothermal Method and the Verification of Crystallization–dissolution–crystallization Mechanism. *J. Mater. Sci. Mater. Electron.* **2014**, *25* (2), 928–935.

(56) Wang, X.; Mao, W.; Zhang, Q.; Wang, Q.; Zhu, Y.; Zhang, J.; Yang, T.; Yang, J.; Li, X.; Huang, W. PVP Assisted Hydrothermal Fabrication and Morphology-Controllable Fabrication of $BiFeO_3$ Uniform Nanostructures with Enhanced Photocatalytic Activities. *J. Alloys Compd.* **2016**, *677*, 288–293.

(57) Joshi, U. A.; Jang, J. S.; Borse, P. H.; Lee, J. S. Microwave Synthesis of Single-Crystalline Perovskite $BiFeO_3$ Nanocubes for Photoelectrode and Photocatalytic Applications. *Appl. Phys. Lett.* **2008**, *92* (24), 242106 (1-3).

(58) Zhu, X.; Hang, Q.; Xing, Z.; Yang, Y.; Zhu, J.; Liu, Z.; Ming, N.; Zhou, P.; Song, Y.; Li, Z.; et al. Microwave Hydrothermal Synthesis, Structural Characterization, and Visible-Light Photocatalytic Activities of Single-Crystalline Bismuth Ferric Nanocrystals. *J. Am. Ceram. Soc.* **2011**, *94* (8), 2688–2693.

(59) Tong, T.; Cao, W.; Zhang, H.; Chen, J.; Jin, D.; Cheng, J. Controllable Phase

Evolution of Bismuth Ferrite Oxides by an Organic Additive Modified Hydrothermal Method. *Ceram. Int.* **2015**, *41* (S1), S106–S110.

(60) Cai, D.; Li, J.; Tong, T.; Jin, D.; Yu, S.; Cheng, J. Phase Evolution of Bismuth Ferrites in the Process of Hydrothermal Reaction. *Mater. Chem. Phys.* **2012**, *134* (1), 139–144.

(61) Wu, L.; Dong, C.; Chen, H.; Yao, J.; Jiang, C.; Xue, D. Hydrothermal Synthesis and Magnetic Properties of Bismuth Ferrites Nanocrystals with Various Morphology. *J. Am. Ceram. Soc.* **2012**, *95* (12), 3922–3927.

(62) Wei, J.; Zhang, C.; Xu, Z. Low-Temperature Hydrothermal Synthesis of $BiFeO_3$ Microcrystals and Their Visible-Light Photocatalytic Activity. *Mater. Res. Bull.* **2012**, *47* (11), 3513–3517.

(63) Fei, L.; Yuan, J.; Hu, Y.; Wu, C.; Wang, J.; Wang, Y. Visible Light Responsive Perovskite $BiFeO_3$ Pills and Rods with Dominant $\{111\}_c$ Facets. *Cryst. Growth Des.* **2011**, *11* (4), 1049–1053.

(64) Li, S.; Lin, Y. H.; Zhang, B. P.; Wang, Y.; Nan, C. W. Controlled Fabrication of $BiFeO_3$ Uniform Microcrystals and Their Magnetic and Photocatalytic Behaviors. *J. Phys. Chem. C* **2010**, *114* (7), 2903–2908.

(65) Mirabbos, H.; Yunhua, X.; Fazhan, W.; Juan, W.; Wengang, L.; Mingqiong, W. Morphology-Controlled Hydrothermal Synthesis of Bismuth Ferrite Using Various Alkaline Mineralizers. *Ceram. - Silikaty* **2009**, *53* (2), 113–117.

(66) Wang, Y.; Xu, G.; Ren, Z.; Wei, X.; Weng, W.; Du, P.; Shen, G.; Han, G. Mineralizer-Assisted Hydrothermal Synthesis and Characterization of $BiFeO_3$ Nanoparticles. *J. Am. Ceram. Soc.* **2007**, *90* (8), 2615–2617.

(67) Gajović, A.; Šturm, S.; JanWar, B.; Šantić, A.; Žagar, K.; Čehz, M. The Synthesis of Pure-Phase Bismuth Ferrite in the Bi-Fe-O System under Hydrothermal Conditions without a Mineralizer. *J. Am. Ceram. Soc.* **2010**, *93* (10), 3173–3179.

(68) Xie, H.; Wang, K.; Jiang, Y.; Zhao, Y.; Wang, X. An Improved Co-Precipitation Method to Synthesize Three Bismuth Ferrites. *Synth. React. Inorganic, Met. Nano-Metal Chem.* **2014**, *44* (9), 1363–1367.

(69) Komarneni, S.; Menon, V. C.; Li, Q. H.; Roy, R.; Ainger, F. Microwave-Hydrothermal Processing of $BiFeO_3$ and $CsAl_2PO_6$. *J. Am. Ceram. Soc.* **1996**, *79* (5), 1409–1412.

(70) Ponzoni, C.; Rosa, R.; Cannio, M.; Buscaglia, V.; Finocchio, E. Optimization of BFO Microwave-Hydrothermal Synthesis : Influence of Process Parameters. *J. Alloys Compd.* **2013**, *558*, 150–159.

(71) Han, S. H.; Kim, K. S.; Kim, H. G.; Lee, H. G.; Kang, H. W.; Kim, J. S.; Cheon, C. Il. Synthesis and Characterization of Multiferroic $BiFeO_3$ Powders Fabricated by Hydrothermal Method. *Ceram. Int.* **2010**, *36* (4), 1365–1372.

(72) Han, J. T.; Huang, Y. H.; Wu, X. J.; Wu, C. L.; Wei, W.; Peng, B.; Huang, W.; Goodenough, J. B. Tunable Synthesis of Bismuth Ferrites with Various Morphologies. *Adv. Mater.* **2006**, *18* (16), 2145–2148.

(73) Wang, Y.; Xu, G.; Yang, L.; Ren, Z.; Wei, X.; Weng, W.; Du, P.; Shen, G.; Han, G. Alkali Metal Ions-Assisted Controllable Synthesis of Bismuth Ferrites by a Hydrothermal Method. *J. Am. Ceram. Soc.* **2007**, *90* (11), 3673–3675.

Chapter 2.

The effects of potassium and sodium cations on the phase and morphology of bismuth iron oxide crystals

2.1 Introduction

The family of materials known as bismuth iron oxides (BFOs) have potential for use in applications ranging from robust data storage and transfer devices[1], to heavy metal adsorption for bioremediation[2], to photocatalysts for the degradation of environmental pollutants[3,4]. However, difficulty in synthesizing single-phase BFOs via traditional means, such as solid-state chemistry, has prompted research in their synthesis under hydrothermal conditions. Hydrothermal synthesis (HTS) makes use of pressure- and heat-tolerant vessels to allow solution-assisted crystal synthesis in a wider range of conditions than are normally possible for aqueous synthesis. Additionally, the use of a solvent in HTS introduces many variables that may be tuned to control phase and morphology outcome. In HTS of BFO, some synthesis variables have included: microwave synthesis[5–8], temperature[9–14], chemical additives/surfactants[6,15–25], and solution chemistry (esp. pH and reactant ratios)[26–30]. Successful synthesis of desired single-phase, morphologically-controlled BFO crystals have even led some groups to hypothesize reaction mechanisms for the formation of specific BFO phases. Unfortunately, there is still no consensus on the mechanism(s) or reaction pathway(s) due to a lack of direct evidence to support proposed reaction steps.

Most reaction sequences proposed in this field have only assumed the formation of soluble, simple complexes of bismuth or iron that react with each other to form the final

products.[7,8,14,20,22,25,31,32] However, a set of neutral-charge, solid intermediates can form before any heat treatment and the formation of the final product. An intermediate crystalline $Bi_{25}FeO_{40}$ phase that seemingly causes the preferential formation of well-defined $BiFeO_3$ crystals was found to form at high temperatures for a very short duration (>180 °C, <1 hour).[10,20,33] Our previous work extended these results by confirming that $Bi_{25}FeO_{40}$ can form at temperatures as low as room-temperature, given enough time (48 hours), and that this room-temperature reaction can occur with initial conditions of low as well as high concentrations of Bi and Fe ions.[34] As a result, reaction sequences proposed in the future will have to take into account the formation of these solid intermediates. Two additional factors also need to be accounted for in proposing reaction pathways: the effects of individual chemical components in solution are largely unknown, and the extent and robustness of these effects under different conditions are unclear. Understanding these two factors is the key to understanding the role of multiple pathways to formation of BFO products.

Spectator ions, ions present in solution that do not react to form the final products, are among the most under-investigated pathway-influencing factors - no proposed reaction sequence for BFOs has taken into account how spectator ions affect the formation of the final products. Debye-Hückel theory and its extensions predict that spectator ions increase the ionic strength in solution, which plays a role in interactions between ions and affects the chemical activity of reacting species. Changes in activity may lead to unexpected changes in the solubility of compounds and equilibria of reactions. At low concentrations, spectator ions only contribute to ionic strength, but at greater concentrations, the chemical identity of the ions becomes important. For

example, recent research in solvothermal synthesis of CdS[35], CdSe[36], and CuInS[37] has shown that the presence of spectator ions can influence the formation of specific phases through a variety of mechanisms. These examples demonstrated that though spectator ions were not part of any reactions to form the final phase, they influenced species who were part of those reactions.

Due to the nature of HTS, every experiment published in this field has used bismuth and iron precursors in the form of oxides or soluble salts, which contain spectator counter-ions, to maintain charge neutrality. There have been reports of spectator ions, specifically cations associated with the OH^- base, influencing the phase outcome of the product.[27,38] However, the cations' effects differ depending on the presence of additives and in different solvents.[19,25] Additionally, there is evidence that the effects of spectator ions extend to crystal morphology control.[18,26–28,39,40] Since the final outcome is the culmination of intermediate steps in a synthesis, studying how spectator ions affect each intermediate result would provide more data to support proposed ion effects and reaction mechanisms. Developing methods to systematically investigate causes and effects at each step of a synthesis would significantly aid understanding of how chemistry affects the solution.

Until now, investigations on the effects of spectator ions on the final product have neglected how spectator ions affect the intermediates. Here, we report our findings on how spectator ions present during the formation of intermediates before and during heat treatment may alter reaction pathways of BFO formation. We show how spectator Na^+ and K^+ ions influence both the intermediate and final products, and under what conditions they affect these precipitates. With the insight gained from previous

experiments on the time-dependent formation of the intermediates before furnace treatment, we developed a versatile, two-step method as a platform for future systematic studies to compare the effects of different spectator ions with respect to this intermediate.

2.2 Experimental

2.2.1 Materials

All reagents were used as received without further purification: Bismuth (III) nitrate pentahydrate (≥98.0%, ACS reagent, Sigma-Aldrich), Iron (III) nitrate nonahydrate (≥98.0%, ACS reagent, Sigma-Aldrich), Potassium hydroxide (~45 wt% (11.7 M) in H_2O, for HPLC, Sigma-Aldrich), Sodium hydroxide (≥98.0%, anhydrous pellets, Sigma-Aldrich), Nitric acid (70%, ACS reagent, Sigma-Aldrich).

2.2.2 Synthesis

Overview: $BiFeO_3$ and $Bi_2Fe_4O_9$ crystals were grown using a HTS method from acidic solutions of bismuth- (Bi^{3+}) and iron- (Fe^{3+}) containing salts reacted with KOH or NaOH base. These solutions were stirred at room temperature to react for a period of time before a final furnace treatment and subsequent washing with water and dilute HNO_3 to remove soluble compounds (*Scheme 2.1)*.

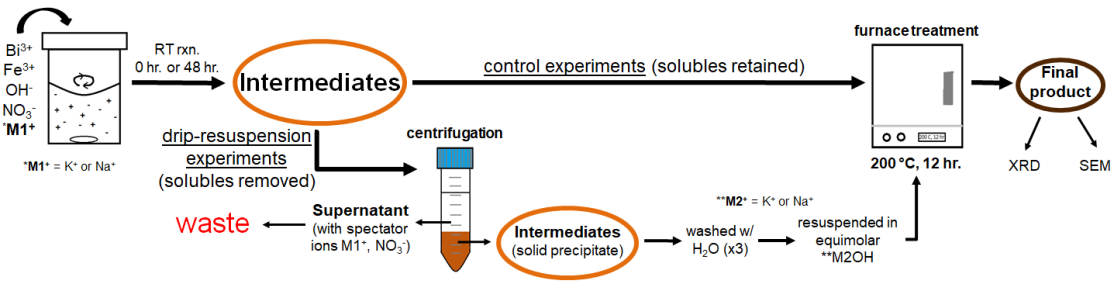

Scheme 2.1: Experimental Overview

Preparation of dissolved metal solution: $Bi(NO_3)_3 \cdot 5H_2O$ and $Fe(NO_3)_3 \cdot 9H_2O$ salts were dissolved in 5 M HNO_3 to make homogeneous solutions of Bi and Fe ions that would be used to make final 80 mL solutions. 10 mM or 100 mM solutions, calculated with respect to the final 80 mL volume, could be made by dissolving different amounts of equimolar quantities of the Bi and Fe salts. To make the 10 mM solution, 0.388 g of Bi salt and 0.323 g of Fe salt were dissolved in 2 mL of 5 M HNO_3. To make the 100 mM solution, 3.881 g of Bi salt and 3.230 g of Fe salt were dissolved in 4 mL of 5 M HNO_3. Resultant acidic solutions were stirred at ~350 rpm and covered with parafilm for a minimum of 1 hour until the salt crystals were completely dissolved. H_2O was added to these acidic solutions so that the total volume was 18 mL per solution. Solutions were stirred for an additional minimum of 10 minutes to equilibrate.

Preparation of intermediate solution: 62 mL of KOH or NaOH solutions were prepared and poured into 80 mL capacity Teflon liners and stirred continuously at 700 rpm. The concentrations of these solutions were prepared such that when subsequently combined with the 18 mL acidic Fe/Bi ions-containing solution, the final 80 mL solution contained 6 M or 9 M $[OH^-]$ concentration, accounting for neutralization with the HNO_3. The acidic metal ions solution was dropwise added by a syringe pump to the stirring base solution at a 0.3 mL/min rate through an 18-gauge needle. The resultant brown intermediate solution was either loaded directly into a Parr bomb or left to react at room temperature for up to 48 hours. If subjected to this room temperature reaction time, samples were covered to prevent water loss and stirred for the duration at 700 rpm. This intermediate solution could be separated for analysis after the room temperature reaction.

The intermediate solution was centrifuged for 5 minutes at 3600 G to isolate the solid brown slurry from the supernatant and the supernatant subsequently poured off. The remaining solid was lyophilized in preparation for XRD and SEM analysis.

Drip-resuspension experiments: After room temperature reaction, the intermediate solution was centrifuged to isolate the solid brown slurry from the supernatant and the supernatant was poured off. The solid slurry was washed three times with water to remove soluble ions. Newly made KOH or NaOH of the same concentration as the original base was introduced back into the slurry. The solution was vortexed to resuspend the solid intermediate in the base and poured back into a Teflon liner. For the drip-resuspension experiments, a distinction is made between the cation on the base used to precipitate out the slurry (denoted M1), and the cation on the base that was reintroduced after washing the slurry (denoted M2). This nomenclature is used in *Scheme 2.1* and later in the text.

Furnace treatment of intermediate solution: The Teflon liner containing the intermediate solution was sealed and loaded into the steel enclosure of a Parr bomb. Once assembled, the Parr bomb was set into a furnace (Thermo Scientific Thermolyne F6028C) at room temperature. The furnace ramped at 1 °C/min to 200 °C, held at 200 °C for 720 minutes, and then allowed to cool naturally to room temperature. The final crystalline products and supernatant solution were poured out of the liner into centrifuge tubes. The products were then washed by a combination of vortexing and centrifuging at 3600 G for 5 min twice in water, twice in 1 M nitric acid, followed by two final

washes with water. The powder and any remaining water was frozen, lyophilized, and prepared for further analysis.

2.2.3 Characterization

Powder X-ray diffraction (XRD) was carried out using a Bruker D8 Advance ECO powder diffractometer with a Cu K-α1 1.54 Å source. Samples were scanned between 12° and 62° in the theta-theta geometry. Patterns were compared with the Joint Committee on Powder Diffraction Standards (JCPDS) database and analyzed with the MDI JADE 9 software package. Samples were considered phase-pure only when there were no other high-intensity diffraction peaks from other phases. Samples were carbon coated using a Denton Desk V sputter coater prior to scanning electron microscopy (SEM) analysis. Sample morphologies were imaged by SEM and energy-dispersive X-ray spectroscopy (EDX) using a Mira3 LM Field Emission Scanning Electron Microscope.

2.3 Results

Overview: Three sets of experiments were conducted - Set A: to compare the effects of K^+ and Na^+ spectator ions on established syntheses of phase-pure bismuth iron oxides; Set B: to determine whether and how the inclusion of either K^+ and Na^+ influenced the formation of a crystalline intermediate; Set C: to determine whether K^+ or Na^+ caused the formation of a special amorphous intermediate with properties that influenced the final phase and morphology. Resultant crystals were also examined and compared to address the morphological implications of our experiments.

Previously, we reported a set of reaction conditions that could be used to selectively synthesize $BiFeO_3$ or $Bi_2Fe_4O_9$ in KOH.[34] Phase-pure $BiFeO_3$ crystals were formed using a 100 mM final metal ion concentration solution in 9 M KOH with the solution allowed to stir and react at room temperature for 48 hours before furnace treatment (*Figure 2.1d (top)*). Phase-pure $Bi_2Fe_4O_9$ was obtained with 10 mM metal ion concentration and 6 M KOH solution and no additional room temperature reaction (*Figure 2.1a (top)*). We developed a shorthand to notate the reaction conditions that will be used in the rest of this paper: (metal ions concentration/final OH^- concentration/room temperature reaction time). Therefore, the reaction conditions that led to $BiFeO_3$ were (100/9/48) while those that led to $Bi_2Fe_4O_9$ were (10/6/0). These results are also summarized in *Figures 2.1a,d*.

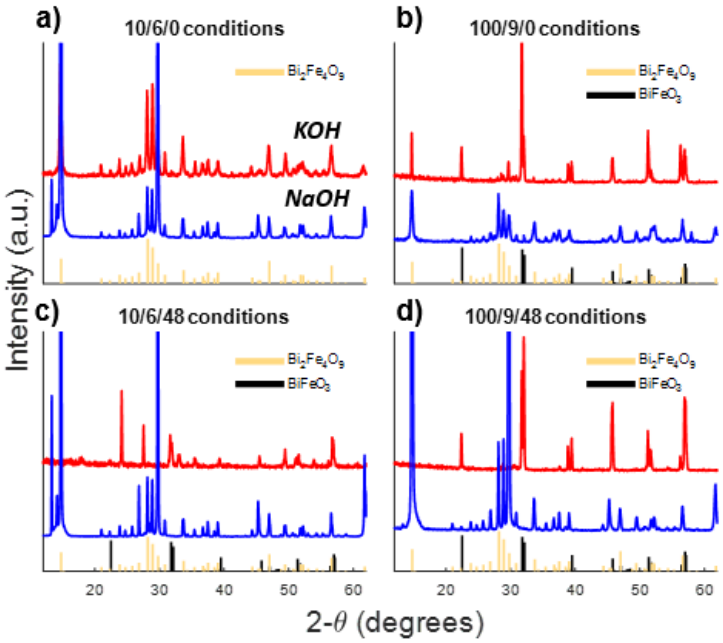

Figure 2.1: XRD patterns of final products of HTS. Conditions are denoted as ([metal ions (mM)]/[OH^- (M)]/room temperature reaction time (hours)). Top (red) line represents solutions reacted with KOH; bottom (blue) line represents solutions reacted with NaOH. a) 10/6/0 conditions produce $Bi_2Fe_4O_9$ in either base. b) 100/9/0 conditions produce a mixed phase of $BiFeO_3$ and $Bi_2Fe_4O_9$ in KOH and only $Bi_2Fe_4O_9$ in NaOH. c) 10/6/48 conditions produce a mixed, majority phase $BiFeO_3$ and minority phase $Bi_2Fe_4O_9$ in KOH; phase-pure $Bi_2Fe_4O_9$ in NaOH. d) 100/9/48 conditions produce phase-pure $BiFeO_3$ in KOH and phase-pure $Bi_2Fe_4O_9$ in NaOH.

In experiment Set A, we studied the effects of instead using NaOH and compared them against the KOH results (*Figure 2.1*). KOH results are presented as the top, red spectrum in each panel while NaOH results are presented as the bottom, blue spectra. Under 10/6/0 conditions (*Figure 2.1a*), the final phase is the same with either KOH or NaOH – $Bi_2Fe_4O_9$. However, for 100/9/48 conditions (*Figure 2.1d*), K^+ leads to $BiFeO_3$ formation while Na^+ leads to $Bi_2Fe_4O_9$ formation. In fact, regardless of what KOH solutions produced, using NaOH always resulted in phase-pure $Bi_2Fe_4O_9$ at all tested conditions. Additionally, there is no clear relationship between the 48 hour room temperature reaction time and the final products when Na^+ was present, while with K^+, the room temperature reaction seemed to be beneficial for formation of $BiFeO_3$.[33,34]

From the results of experiment Set A, we conclude that Na^+ prefers the formation of only one phase – $Bi_2Fe_4O_9$ – under all tested conditions. However, previous research suggests that the concentrations of metal ions and base that we used may not be diverse enough to allow the formation of other phases, as other groups were able to synthesize $BiFeO_3$ using NaOH.[7,25] We made two hypotheses about the role of the base cations in synthesis. Our first hypothesis was that the cations influenced the formation of certain intermediate products which promote or inhibit the nucleation of final phases. Our second hypothesis was that the cations' presence in solution was the only requirement for the formation of certain final phases. The next sets of experiments sought to explore both of these possibilities.

To test our first hypothesis, we designed experiment Set B. In this experiment, we analyzed the solid intermediate formed after reaction with base but before furnace treatment. Under 10/6/0 conditions, an amorphous brown slurry formed regardless of

the base used (*Figure 2.2a*). In contrast, 100/9/48 conditions caused the formation of a crystalline $Bi_{25}FeO_{40}$ intermediate (*Figure 2.2d*). Amorphous intermediates formed under 100/9/0 conditions, similar to that of 10/6/0 conditions, but with an unidentified crystalline intermediate in KOH (*Figure 2.2b*). The presence of an amorphous phase is more apparent in the 10/6/48 spectra than in the 100/9/48 spectra, though both conditions appear to produce very well-defined $Bi_{25}FeO_{40}$ peaks. The absence of $Bi_{25}FeO_{40}$ with the 10/6/0 and 100/9/0 conditions (*Figures 2.2a,b*) compared to that of the 48 hour conditions (*Figures 2.2c,d*) suggests that the formation of this crystalline intermediate is due solely to the room temperature reaction, confirming previous reports.[33,34] Differences appear to be negligible between intermediates in different bases as indicated by the results - primarily amorphous product without room temperature

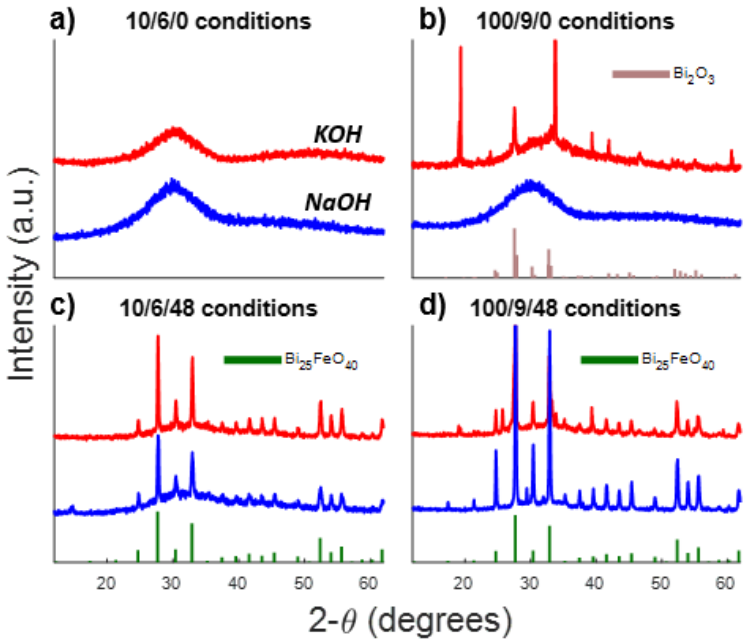

Figure 2.2: XRD patterns of the intermediate products of HTS. Conditions and line colors are the same as for Figure 2.1 experiments. a) 10/6/0 conditions produce amorphous products in either base. It is unclear whether both products are the same. b) 100/9/0 conditions produce a mix of amorphous and unidentified crystalline product in KOH; only amorphous product in NaOH. c) 10/6/48 conditions produce a mix of amorphous product and crystalline $Bi_{25}FeO_{40}$ in either base. d) 100/9/48 conditions produce the same mix of amorphous and $Bi_{25}FeO_{40}$ phases as in c) for both bases.

reaction and the presence of crystalline $Bi_{25}FeO_{40}$ with room temperature reaction. The nearly identical spectra in either base suggest that the cations do not affect the formation of the intermediate.

Before exploring the role of cations during the furnace treatment, we tried to better understand how the composition of the intermediate influences the final phase. Room temperature reaction causes crystalline $Bi_{25}FeO_{40}$ to form in either base (*Figure 2.2*), but leads to the formation of $BiFeO_3$ in KOH and $Bi_2Fe_4O_9$ in NaOH (*Figure 2.1*). XRD only confirmed that the cations did not affect the formation of crystalline intermediates; we gained no knowledge about the identity of the amorphous component. Therefore, we developed a method (Set C) to explore the effects and incorporation of cations on the amorphous intermediates. With this method, we sought to determine whether the amorphous intermediates, rather than the crystalline intermediate, influenced the final products that form.

"Drip-resuspension" experiments (in experiment Set C) were developed by splitting the usual synthesis procedures into two main steps (both described in **Methods** and summarized in *Scheme 2.1*). The first step involves precipitating the intermediates by adding base. If cations affect the development of the amorphous component of the intermediates, kinetics could also be affected. Since we wanted to understand whether the intermediate composition affected the final product, we needed to avoid the possibility that the intermediates were not done transforming before moving on to the second step. The experiments would have to be conducted under conditions that allowed time for equilibration, leaving 10/6/48 and 100/9/48 conditions as candidates. Of these two conditions, only 100/9/48 could produce phase-pure BFOs (*Figures 2.1c,d*), which

was an important consideration to be able to correlate the intermediates to a final product. Additionally, changes in the final phases would be easier to detect with a single phase than with mixed phases. Thus, these experiments used only 100/9/48 conditions to allow qualitative correlation of a known intermediate slurry composition to an expected final product.

The second step of this method involves separating the intermediate precipitates from the supernatant containing soluble spectator ions and then replacing the supernatant with an equivalent amount of new base. Using this method, we previously discovered that the majority of the Fe in the intermediate solution is incorporated into either $Bi_{25}FeO_{40}$ or the amorphous intermediate rather than being dissolved.[34] This result demonstrated that the drip-resuspension method is effective for retaining insoluble compounds and washing away only soluble spectator ions (e.g. K^+, Na^+, NO_3^-), allowing us to compare the individual effects of high amounts of K^+ and Na^+ in solution at will (assuming these ions are not incorporated into the intermediate in significant amounts). After washing the solid intermediate, we replaced the supernatant with new, equimolar base to restore the original solution conditions, minus soluble spectator ions.

The results of the drip-resuspension experiments are presented in *Figure 2.3*. We use the shorthand M1 and M2 to indicate the cation, either K^+ or Na^+, on the base used during the first and second respective steps in these experiments. When the intermediate is precipitated out by KOH (M1 = K^+), washed of spectator ions, and then furnace reacted in new KOH (M2 = K^+), we observe that only $BiFeO_3$ is formed (*Figure 2.3a*). For M1 = M2 = Na^+, we see that $Bi_2Fe_4O_9$ and $Bi_{25}FeO_{40}$ form instead of $BiFeO_3$ (*Figure 2.3d*). These spectra match the results without drip-resuspension (*Figure 2.1d*), except

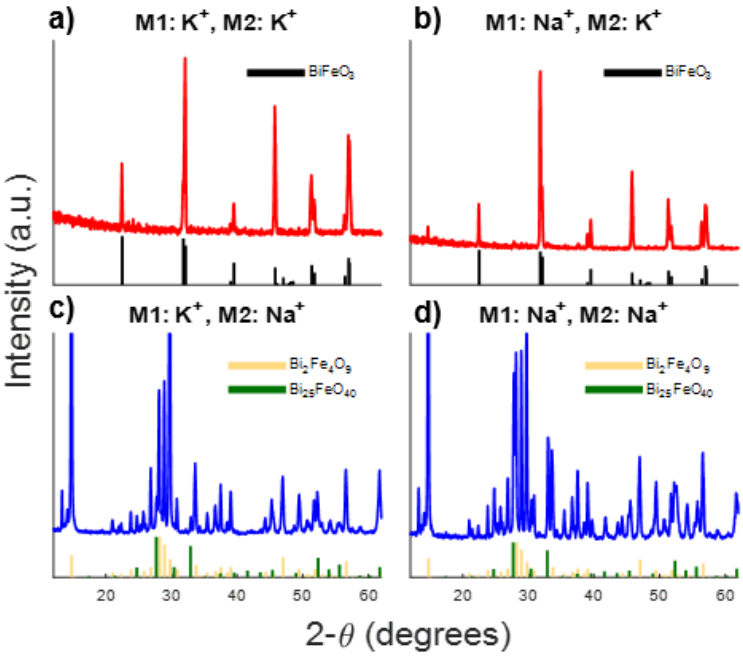

Figure 2.3: XRD patterns for the final products of the drip-resuspension experiments (100/9/48 conditions). M1 indicates the cation on the base used to precipitate the intermediates, while M2 indicates the cation used after washing and during furnace reaction (Scheme 2.1). For all experiments, the M1 base is replaced by a newly prepared M2 base of the same concentration. a) M1 = M2 = K^+; phase-pure $BiFeO_3$. b) M1 = Na^+, M2 = K^+; phase-pure $BiFeO_3$. c) M1 = K^+, M2 = Na^+; phase-pure $Bi_2Fe_4O_9$. d) M1 = M2 = Na^+; phase-pure $Bi_2Fe_4O_9$.

with the surprising result that $Bi_{25}FeO_{40}$ was also present in the final products after drip-resuspension. When M1 = Na^+ and M2 = K^+, $BiFeO_3$ is formed (*Figure 2.3b*). When M1 = K^+ and M2 = Na^+, $Bi_2Fe_4O_9$ and $Bi_{25}FeO_{40}$ are formed (*Figure 2.3c*). As the final phases are the same for the experiments with matching M2, the determining factor for the final phase selection appears to be the spectator cation present in the final solution.

Up to this point, we have focused on the effects of spectator ions on phase control. Controlling crystal phases is the only way to guarantee access to desired properties of materials. Spectator ions are a promising path to obtaining specific phases of BFOs under a wide range of conditions. However, morphologies of crystals can affect properties at the nanoscale and may also be affected by spectator ion inclusion. Therefore, we sought to understand the effects of spectator ions on the morphologies of

BFO crystals. The morphologies of final products obtained at 100/9/48 conditions are depicted in *Figure 2.4*. The K^+ column (left) depicts images of $BiFeO_3$ while the Na^+ column (right) depicts images of $Bi_2Fe_4O_9$ and impurity $Bi_{25}FeO_{40}$.

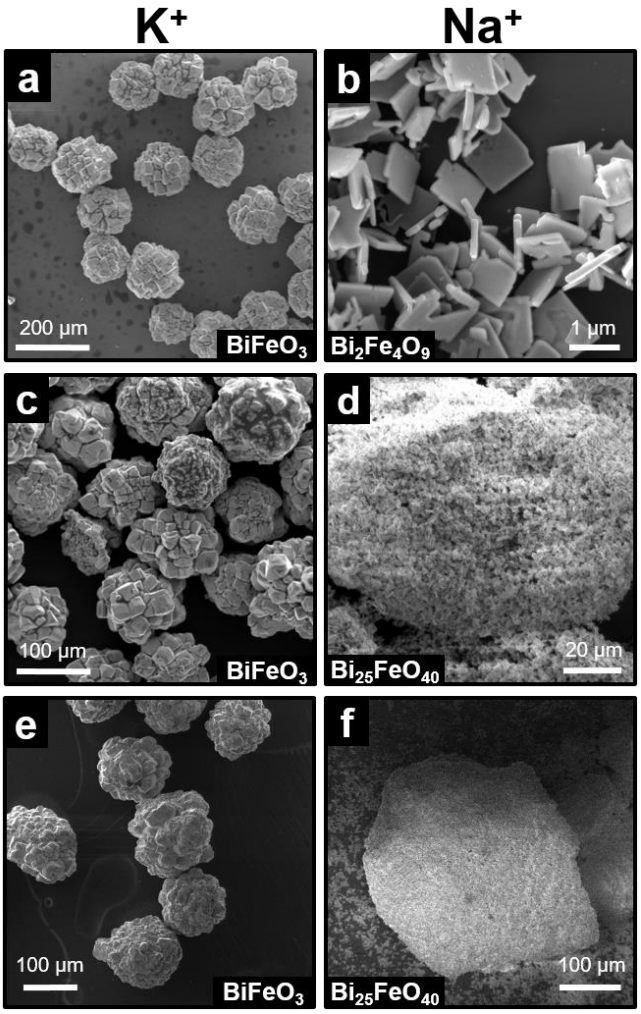

Figure 2.4: SEM images of representative morphologies of final products. Unless otherwise elaborated, these crystals were synthesized in a solution containing the cation denoted at the top. The top row depicts crystals synthesized with no drip-resuspension (Figure 2.1d*)*. The middle row depicts crystals synthesized with drip-resuspension, where M1 = M2 (Figures 2.3a,d). The bottom row depicts crystals synthesized with drip-resuspension, where M1 ≠ M2, and M2 is the cation denoted at the top (Figures 2.3b,c). *(e)* and *(f)* are the impurity $Bi_{25}FeO_{40}$ present among $Bi_2Fe_4O_9$ crystals (Figures 2.3c,d). All crystals were synthesized under 100/9/48 conditions.

In both cases, the morphology is that of crystal blocks made of cube-like constituent crystallites. $BiFeO_3$ crystals are more well-defined when the intermediate is not

resuspended than when it is resuspended (*Figure 2.4a* vs. *Figures 2.4c,e*). There appears to be a correlation between loss of facet definition in the constituent cubes and washing away spectator anions, suggesting a role in crystal growth for anions. There has been no other work in this field yet to confirm that spectator anions independently contribute to crystal formation. Additionally, the $BiFeO_3$ crystals do not vary whether the intermediate was precipitated in NaOH or KOH (i.e. M1 = Na^+ or K^+), supporting our hypothesis that the cations play a role only during the furnace treatment stage (*Figures 2.4c,e*).

Phase-pure $Bi_2Fe_4O_9$ in the *Figure 2.1* experiments crystallized into sheet morphologies typical of $Bi_2Fe_4O_9$ crystals formed by HTS[27,38,41,42] (*Figure 2.4a*). Ill-defined, large structures are characteristic of $Bi_{25}FeO_{40}$ crystals formed by HTS[20,33,43] (*Figures 2.4d,f)*. Energy dispersive X-ray spectroscopy (EDX) scans of representative areas of the ill-defined crystals indicate a Bi:Fe:O ratio of 25:10:40 (*Appendix Figure S1*). As these EDX scans were not taken of flat, polished samples, this data may be unreliable for more than an approximation of the elemental ratios. However, it is possible that the deviation of Fe from the ideal 25:1:40 ratio is due to $Bi_2Fe_4O_9$ crystals nucleating on background $Bi_{25}FeO_{40}$, and that given longer heating times, more phase-characteristic shapes would become distinguishable. In general, when both $Bi_2Fe_4O_9$ and $Bi_{25}FeO_{40}$ form in the drip-resuspension experiments, crystal definition is lost, making it impossible to visually distinguish one phase from another despite XRD spectra indicating that two separate crystalline phases are present. As a result of the impurity $Bi_{25}FeO_{40}$ crystals, no conclusions can be drawn about the effects of spectator cations on crystal morphology (*Figures 2.4d,f*).

2.4 Discussion

Based upon the 3 Sets of experiments (A-C), we conclude that the final phase is decided by the spectator cation species present during heat treatment rather than the base cations forming special intermediates that lead to formation of certain final products. Interestingly, for the experiments with resuspension in NaOH ($M2 = Na^+$), $Bi_{25}FeO_{40}$ formed in addition to the expected $Bi_2Fe_4O_9$. $Bi_{25}FeO_{40}$ usually decomposes during furnace treatment to give way to either $BiFeO_3$ or $Bi_2Fe_4O_9$ (*Figure 2.2*). In this case, why was $Bi_{25}FeO_{40}$ present in the final products? Was it left over from the intermediate or did it dissolve and then reprecipitate again? If $Bi_2Fe_4O_9$ formed via solid-state transformation from the intermediates, the iron-rich amorphous intermediate would be completely consumed before the $Bi_{25}FeO_{40}$ was used up due to the 1:2 ratio of Bi:Fe in $Bi_2Fe_4O_9$. Then, the $Bi_{25}FeO_{40}$ in the final product could plausibly be untransformed intermediate $Bi_{25}FeO_{40}$. If $Bi_{25}FeO_{40}$ first dissolved instead, Bi^{3+} would be released into the solution. $Bi_2Fe_4O_9$ would form followed by $Bi_{25}FeO_{40}$ reforming due to a remaining excess of Bi^{3+} (whereas in the case of $BiFeO_3$ formation, there is no excess Bi^{3+} relative to Fe^{3+} and thus no $Bi_{25}FeO_{40}$). Neither of these mechanisms can be disproven with the drip-resuspension data. However, in conjunction with the *Figure 2.1* data, we posit the likelihood of the dissolution-reprecipitation mechanism.

The difference between the products of Na^+ experiments in *Figure 2.1d* and in *Figures 2.3c,d* is the presence of $Bi_{25}FeO_{40}$ in the latter. The only difference in reaction conditions between these sets of experiments is the lack of NO_3^- spectator ions in the drip-resuspension experiments. Spectator ions contribute to the ionic strength in a solution, which can influence activity. However, a calculation of the ionic strengths

between our system with and without NO_3^- counter-ion (using the 100/9/48 conditions) shows only a 3% difference (*Appendix S2*). Although it is possible that this minor difference in ionic strength is the cause of the differences seen in these experiments, it may be worth considering that spectator ions have a more specific role in synthesis, such as stabilization of Bi^{3+}, Fe^{3+}, and their complexes and compounds. We conjecture that if NO_3^- stabilizes Bi and Fe ions, $Bi_{25}FeO_{40}$ is less likely to form. Without stabilization by NO_3^-, Bi and Fe ions would be less soluble, resulting in a greater relative supersaturation for a given concentration in solution. Their supersaturation would drive the formation of precursor complexes that would then react to form crystals of $Bi_{25}FeO_{40}$. Thus, less NO_3^- would result in formation of $Bi_{25}FeO_{40}$.

We considered combinations of our NO_3^- stabilization hypothesis with a solid-state transformation or dissolution-reprecipitation mechanism in a set of thought experiments (*Table 2.1*). A combination would be plausible if it matched all of our given data. In

Table 2.1: $Bi_2Fe_4O_9$ and $Bi_{25}FeO_{40}$ formation mechanism hypotheses

A) If NO_3^- stabilizes Bi^{3+}/Fe^{3+} ions & solid-state transformation occurs
NDR: $Bi_2Fe_4O_9$ forms, untransformed $Bi_{25}FeO_{40}$ remains
DR: $Bi_2Fe_4O_9$ forms, untransformed $Bi_{25}FeO_{40}$ remains
Conclusion: contradicts data
B) If NO_3^- stabilizes Bi^{3+}/Fe^{3+} ions & dissolution-reprecipitation occurs
NDR: $Bi_{25}FeO_{40}$ dissolves and only $Bi_2Fe_4O_9$ forms
DR: $Bi_{25}FeO_{40}$ dissolves, $Bi_2Fe_4O_9$ forms, $Bi_{25}FeO_{40}$ reforms from remaining ions
Conclusion: plausible
C) If NO_3^- contributes only to ionic strength & solid-state transformation occurs
NDR: $Bi_2Fe_4O_9$ forms, untransformed $Bi_{25}FeO_{40}$ remains
DR: same result as NDR
Conclusion: contradicts data
D) If NO_3^- contributes only to ionic strength & dissolution-reprecipitation occurs
NDR: $Bi_{25}FeO_{40}$ dissolves, $Bi_2Fe_4O_9$ forms, $Bi_{25}FeO_{40}$ reforms if it is energetically favorable for it to do so
DR: same result as NDR
Conclusion: contradicts data
Key: NDR = not drip-resuspended; DR = drip-resuspended

"NO_3^- stabilizes Bi^{3+}/Fe^{3+} ions" cases, NO_3^- is present in non-drip-resuspended experiments (NDR in the table; corresponds to *Figure 2.1* data) while it is not in drip-resuspended experiments (DR in the table; corresponds to *Figure 2.3* data). In the "NO_3^- contributes only to ionic strength" cases, NO_3^- is presumed to only contribute to ionic strength with no other effects, leading to the same results between experiments. $BiFeO_3$ formation was not included in these thought experiments because every combination presented would lead to phase-pure $BiFeO_3$ due to its equimolar Bi:Fe ratio (assuming $BiFeO_3$ and $Bi_2Fe_4O_9$ would be more likely to form than $Bi_{25}FeO_{40}$ during heat treatment).

In Case A, $Bi_2Fe_4O_9$ forms from the intermediate and eventually exhausts its Fe^{3+} source, leaving behind Bi ions in the form of untransformed $Bi_{25}FeO_{40}$ crystals. With or without NO_3^-, $Bi_{25}FeO_{40}$ is not expected to dissolve after $Bi_2Fe_4O_9$ formation, thus making the results identical between these two experiments. However, these hypothetical results are in disagreement with our data, and so we can rule out this combination. In Case B, $Bi_{25}FeO_{40}$ dissolves first, leaving behind free Bi ions or complexes. After $Bi_2Fe_4O_9$ forms, Fe ions remaining after equilibrium combine with excess Bi ions to form $Bi_{25}FeO_{40}$ again. Only without NO_3^- is the supersaturation threshold lowered enough to nucleate out $Bi_{25}FeO_{40}$. These results are what we observe, making this combination plausible. In Case C, NO_3^- has no effect, meaning both hypothetical experiments have the same outcome. The reaction sequences are otherwise the same as for Case A. As these results are not what we observe, this combination is infeasible. In Case D, similar to Case B, $Bi_2Fe_4O_9$ forms but $Bi_{25}FeO_{40}$ only forms if it is favorable to do so, which cannot be predicted if NO_3^- has no stabilizing effect. But as

both experiments should have the same outcome due to NO_3^- doing nothing, both experiments either form only $Bi_2Fe_4O_9$ or both $Bi_2Fe_4O_9$ and $Bi_{25}FeO_{40}$. These results are not supported by our data.

Using process of elimination on our thought experiments in conjunction with our data suggests the stabilization effects of NO_3^- on Bi^{3+} and Fe^{3+} (Case B). Stabilization explains why $Bi_{25}FeO_{40}$ does form after furnace treatment in drip-resuspended samples. Furthermore, this reasoning suggests that $Bi_2Fe_4O_9$ forms via dissolution-reprecipitation. Although NO_3^- stabilization is compatible with our $BiFeO_3$ data, our current data is not sufficient for us to be able to suggest a formation mechanism for $BiFeO_3$. Nonetheless, the drip-resuspension process allowed us to infer the effects of NO_3^- on reaction mechanisms without the use of more sophisticated techniques. With minor modifications, this method could enable the study of other counter-anions as well.

2.5 Conclusions and Future Work

In this work, we compared the effects of Na^+ and K^+ base counter-ions on the intermediate products formed before furnace treatment and on the final bismuth iron oxide products formed after. In particular, we observed that under all of the conditions tested, synthesis in NaOH preferentially forms $Bi_2Fe_4O_9$, while formed final phases varied in KOH. To understand whether these cations were affecting the formation of an intermediate that influenced the formation of the final phases, we stopped our syntheses halfway to investigate the intermediates precipitated out by both bases. The general composition of the intermediates did not vary much between bases under all tested conditions. A 48-hour room temperature reaction appeared to be the only factor for

determining whether a crystalline $Bi_{25}FeO_{40}$ phase formed in addition to an amorphous phase in the intermediate. Due to the limitations of powder x-ray diffraction, we were not able to characterize changes in the amorphous products between bases. To reveal whether changes in the amorphous intermediates were causing a difference in the final products, we developed a method to investigate the effects that the cations have on the intermediate products. Our "drip-resuspension" method allowed us to select the cations present during formation of the intermediates and the final products. The drip-resuspension experiments revealed that only the cation present during formation of the final products (during furnace treatment) dictated the final phases, regardless of the base used to precipitate out the intermediate. When K^+ was present during the furnace treatment, $BiFeO_3$ resulted. When Na^+ was present during the furnace treatment, $Bi_2Fe_4O_9$ and impurity $Bi_{25}FeO_{40}$ resulted. The unexpected presence of $Bi_{25}FeO_{40}$ in the final phase of the drip-resuspension experiments allowed us to conjecture a stabilization role for NO_3^- spectator ions. We reasoned that if NO_3^- stabilizes Bi and Fe ions, $Bi_2Fe_4O_9$ forms by a dissolution-reprecipitation mechanism. NO_3^- stability is also compatible with our $BiFeO_3$ data, but we could not extend our reasoning to infer a formation mechanism for $BiFeO_3$. Finally, we investigated the effects of spectator ions on crystal morphology. We noticed a small loss of facet definition for $BiFeO_3$ crystals prepared by drip-resuspension versus those prepared without. Without drip-resuspension, $Bi_2Fe_4O_9$ took the form of thin, rectangular plates. Comparatively, $Bi_2Fe_4O_9$ crystals in the $Bi_2Fe_4O_9$ and $Bi_{25}FeO_{40}$ mixture produced by drip-resuspension suffered from severe degradation in crystal definition to the point that they were visually indistinguishable from the aggregated masses of $Bi_{25}FeO_{40}$. Due to the loss of crystal

definition, we were not able to draw any conclusions on the effects of spectator cations on crystal morphology.

Future work would expand the use of this method to elucidate the functions of the most commonly used spectator ions (i.e. Li^+, Na^+, K^+, NO_3^-, Cl^-). Although our results indicated that K^+ and Na^+ do not affect the formation of the intermediates, we do not know how more substantial concentrations of spectator anions or other cations will affect it. New intermediates give rise to the possibility of more spectator ion-dependent reaction pathways, making important an understanding of whether mixing spectator ions is simply additive of their effects. If ion combinations show promise of phase and morphology control, property-tailored BFO crystals would be attainable through mild conditions requiring only reusable ions. In turn, the facile synthesis of such crystals would encourage the hydrothermal synthesis of other materials that present a competition between phases that are similar in energy and stabilities.

2.6 References

(1) Catalan, G.; Scott, J. F. Physics and Applications of Bismuth Ferrite. *Adv. Mater.* **2009**, *21* (24), 2463–2485.

(2) Kong, M.; Song, H.; Li, F.; Dai, D.; Gao, H. Facile Synthesis of $Bi_2Fe_4O_9$ Nanoplate and Its Application as a Novel Adsorbent for Cu(II) Removal. *J. Environ. Chem. Eng.* **2017**, *5* (1), 69–78.

(3) Dai, Y.; Yin, L. Low Fe-Doped Bi_2O_3 Photocatalyst with Long Wavelength Response: Crystalline Transition and Mechanisms by First-Principles Calculation. *J. Alloys Compd.* **2013**, *563*, 80–84.

(4) Köferstein, R.; Buttlar, T.; Ebbinghaus, S. G. Investigations on $Bi_{25}FeO_{40}$ Powders Synthesized by Hydrothermal and Combustion-like Processes. *J. Solid State Chem.* **2014**, *217*, 50–56.

(5) Komarneni, S.; Menon, V. C.; Li, Q. H.; Roy, R.; Ainger, F. Microwave-Hydrothermal Processing of $BiFeO_3$ and $CsAl_2PO_6$. *J. Am. Ceram. Soc.* **1996**, *79* (5), 1409–1412.

(6) Joshi, U. A.; Jang, J. S.; Borse, P. H.; Lee, J. S. Microwave Synthesis of Single-Crystalline Perovskite $BiFeO_3$ Nanocubes for Photoelectrode and Photocatalytic Applications. *Appl. Phys. Lett.* **2008**, *92* (24), 242106 (1-3).

(7) Li, S.; Nechache, R.; Davalos, I. A. V.; Goupil, G.; Nikolova, L.; Nicklaus, M.; Laverdiere, J.; Ruediger, A.; Rosei, F. Ultrafast Microwave Hydrothermal Synthesis of $BiFeO_3$ Nanoplates. *J. Am. Ceram. Soc.* **2013**, *96* (10), 3155–3162.

(8) Ponzoni, C.; Rosa, R.; Cannio, M.; Buscaglia, V.; Finocchio, E. Optimization of BFO Microwave-Hydrothermal Synthesis : Influence of Process Parameters. *J. Alloys Compd.* **2013**, *558*, 150–159.

(9) Chen, C.; Cheng, J.; Yu, S.; Che, L.; Meng, Z. Hydrothermal Synthesis of Perovskite Bismuth Ferrite Crystallites. *J. Cryst. Growth* **2006**, *291* (1), 135–139.

(10) Chen, X. Z.; Qiu, Z. C.; Zhou, J. P.; Zhu, G.; Bian, X. B.; Liu, P. Large-Scale Growth and Shape Evolution of Bismuth Ferrite Particles with a Hydrothermal

Method. *Mater. Chem. Phys.* **2011**, *126* (3), 560–567.

(11) Qiu, Z. C.; Zhou, J. P.; Zhu, G.; Chen, X. Z.; Chen, X. M.; Liu, P. Hydrothermal Synthesis of Perovskite Bismuth Ferrite Crystallites with the Help of NH4Cl. *Proc. - 2010 8th Int. Vac. Electron Sources Conf.* **2010**, *2*, 482–483.

(12) Zhang, H.; Kajiyoshi, K. Hydrothermal Synthesis and Size-Dependent Properties of Multiferroic Bismuth Ferrite Crystallites. *J. Am. Ceram. Soc.* **2010**, *93* (11), 3842–3849.

(13) Yan, D.; Sun, C.; Jian, J.; Sun, Y.; Wu, R.; Li, J. Structure and Phase Transition of $BiFeO_3$ Particles Prepared by Hydrothermal Method and the Verification of Crystallization–dissolution–crystallization Mechanism. *J. Mater. Sci. Mater. Electron.* **2014**, *25* (2), 928–935.

(14) Xu, X.; Xu, Q.; Huang, Y.; Hu, X.; Huang, Y.; Wang, G.; Hu, X.; Zhuang, N. Control of Crystal Phase and Morphology in Hydrothermal Synthesis of $BiFeO_3$ Crystal. *J. Cryst. Growth* **2016**, *437*, 42–48.

(15) Chen, Z.; Jin, W. Low-Temperature Acetone-Assisted Hydrothermal Synthesis and Characterization of $BiFeO_3$ Powders. *J. Mater. Sci. Mater. Electron.* **2014**, *25* (9), 4039–4045.

(16) Qiu, Z. C.; Zhou, J. P.; Zhu, G.; Chen, X. Z.; Chen, X. M.; Liu, P. Hydrothermal Synthesis of Perovskite Bismuth Ferrite Crystallites with the Help of NH_4Cl. *J. Nanoparticle Res.* **2012**, *12* (8), 6552–6557.

(17) Wang, X.; Mao, W.; Zhang, Q.; Wang, Q.; Zhu, Y.; Zhang, J.; Yang, T.; Yang, J.; Li, X.; Huang, W. PVP Assisted Hydrothermal Fabrication and Morphology-Controllable Fabrication of $BiFeO_3$ Uniform Nanostructures with Enhanced Photocatalytic Activities. *J. Alloys Compd.* **2016**, *677*, 288–293.

(18) Zhu, X.; Hang, Q.; Xing, Z.; Yang, Y.; Zhu, J.; Liu, Z.; Ming, N.; Zhou, P.; Song, Y.; Li, Z.; et al. Microwave Hydrothermal Synthesis, Structural Characterization, and Visible-Light Photocatalytic Activities of Single-Crystalline Bismuth Ferric Nanocrystals. *J. Am. Ceram. Soc.* **2011**, *94* (8), 2688–2693.

(19) Tong, T.; Cao, W.; Zhang, H.; Chen, J.; Jin, D.; Cheng, J. Controllable Phase

Evolution of Bismuth Ferrite Oxides by an Organic Additive Modified Hydrothermal Method. *Ceram. Int.* **2015**, *41* (S1), S106–S110.

(20) Cai, D.; Li, J.; Tong, T.; Jin, D.; Yu, S.; Cheng, J. Phase Evolution of Bismuth Ferrites in the Process of Hydrothermal Reaction. *Mater. Chem. Phys.* **2012**, *134* (1), 139–144.

(21) Wu, L.; Dong, C.; Chen, H.; Yao, J.; Jiang, C.; Xue, D. Hydrothermal Synthesis and Magnetic Properties of Bismuth Ferrites Nanocrystals with Various Morphology. *J. Am. Ceram. Soc.* **2012**, *95* (12), 3922–3927.

(22) Wei, J.; Zhang, C.; Xu, Z. Low-Temperature Hydrothermal Synthesis of $BiFeO_3$ Microcrystals and Their Visible-Light Photocatalytic Activity. *Mater. Res. Bull.* **2012**, *47* (11), 3513–3517.

(23) Fei, L.; Yuan, J.; Hu, Y.; Wu, C.; Wang, J.; Wang, Y. Visible Light Responsive Perovskite $BiFeO_3$ Pills and Rods with Dominant $\{111\}_c$ Facets. *Cryst. Growth Des.* **2011**, *11* (4), 1049–1053.

(24) Li, S.; Lin, Y. H.; Zhang, B. P.; Wang, Y.; Nan, C. W. Controlled Fabrication of $BiFeO_3$ Uniform Microcrystals and Their Magnetic and Photocatalytic Behaviors. *J. Phys. Chem. C* **2010**, *114* (7), 2903–2908.

(25) Mirabbos, H.; Yunhua, X.; Fazhan, W.; Juan, W.; Wengang, L.; Mingqiong, W. Morphology-Controlled Hydrothermal Synthesis of Bismuth Ferrite Using Various Alkaline Mineralizers. *Ceram. - Silikaty* **2009**, *53* (2), 113–117.

(26) Zhou, M.; Li, W.; Du, Y.; Kong, D.; Wang, Z.; Meng, Y.; Sun, X.; Yan, T.; Kong, D.; You, J. Hydrothermal Synthesis of Bismuth Ferrite Fenton-like Catalysts and Their Properties. *J. Nanoparticle Res.* **2016**, *18* (11), 346 (1-15).

(27) Tsai, C. J.; Yang, C. Y.; Liao, Y. C.; Chueh, Y. L. Hydrothermally Grown Bismuth Ferrites: Controllable Phases and Morphologies in a Mixed KOH/NaOH Mineralizer. *J. Mater. Chem.* **2012**, *22* (34), 17432–17436.

(28) Wang, Y.; Xu, G.; Ren, Z.; Wei, X.; Weng, W.; Du, P.; Shen, G.; Han, G. Mineralizer-Assisted Hydrothermal Synthesis and Characterization of $BiFeO_3$ Nanoparticles. *J. Am. Ceram. Soc.* **2007**, *90* (8), 2615–2617.

(29) Gajović, A.; Šturm, S.; JanWar, B.; Šantić, A.; Žagar, K.; Čehz, M. The Synthesis of Pure-Phase Bismuth Ferrite in the Bi-Fe-O System under Hydrothermal Conditions without a Mineralizer. *J. Am. Ceram. Soc.* **2010**, *93* (10), 3173–3179.

(30) Xie, H.; Wang, K.; Jiang, Y.; Zhao, Y.; Wang, X. An Improved Co-Precipitation Method to Synthesize Three Bismuth Ferrites. *Synth. React. Inorganic, Met. Nano-Metal Chem.* **2014**, *44* (9), 1363–1367.

(31) Han, S. H.; Kim, K. S.; Kim, H. G.; Lee, H. G.; Kang, H. W.; Kim, J. S.; Cheon, C. Il. Synthesis and Characterization of Multiferroic $BiFeO_3$ Powders Fabricated by Hydrothermal Method. *Ceram. Int.* **2010**, *36* (4), 1365–1372.

(32) Li, J.; Yan, D. Z. Low-Temperature Synthesis of Pure $BiFeO_3$ Phase and Variation in Its Morphology with Temperature. *Ceram. Int.* **2018**, *44* (15), 18271–18278.

(33) Lopes, A. M. L.; Araújo, J. P.; Ferdov, S. Room Temperature Synthesis of $Bi_{25}FeO_{39}$ and Hydrothermal Kinetic Relations between Sillenite- and Distorted Perovskite-Type Bismuth Ferrites. *Dalt. Trans.* **2014**, *43* (48), 18010–18016.

(34) Goldman, A. R.; Fredricks, J. L.; Estroff, L. A. Exploring Reaction Pathways in the Hydrothermal Growth of Phase-Pure Bismuth Ferrites. *J. Cryst. Growth* **2017**, *468* (September 2016), 104–109.

(35) Tai, G.; Zhou, J.; Guo, W. Inorganic Salt-Induced Phase Control and Optical Characterization of Cadmium Sulfide Nanoparticles. *Nanotechnology* **2010**, *21* (17), 175601 (1-7).

(36) Lim, J.; Bae, W. K.; Park, K. U.; Zur Borg, L.; Zentel, R.; Lee, S.; Char, K. Controlled Synthesis of CdSe Tetrapods with High Morphological Uniformity by the Persistent Kinetic Growth and the Halide-Mediated Phase Transformation. *Chem. Mater.* **2013**, *25* (8), 1443–1449.

(37) Yu, C.; Zhang, L.; Tian, L.; Liu, D.; Chen, F.; Wang, C. Synthesis and Formation Mechanism of $CuInS_2$ Nanocrystals with a Tunable Phase. *CrystEngComm* **2014**, *16* (41), 9596–9602.

(38) Wang, Y.; Xu, G.; Yang, L.; Ren, Z.; Wei, X.; Weng, W.; Du, P.; Shen, G.; Han,

G. Alkali Metal Ions-Assisted Controllable Synthesis of Bismuth Ferrites by a Hydrothermal Method. *J. Am. Ceram. Soc.* **2007**, *90* (11), 3673–3675.

(39) Du, Y.; Cheng, Z.; Dou, S.; Wang, X. Tunable Morphology and Magnetic Properties of $Bi_2Fe_4O_9$ Nanocrystal Synthesized by Hydrothermal Method. *J. Nanosci. Nanotechnol.* **2011**, *11* (3), 2691–2695.

(40) Liu, Y.; Zuo, R. Morphology and Optical Absorption of $Bi_2Fe_4O_9$ Crystals via Mineralizer-Assisted Hydrothermal Synthesis. *Particuology* **2013**, *11* (5), 581–587.

(41) Zhang, X.; Lv, J.; Bourgeois, L.; Cui, J.; Wu, Y.; Wang, H.; Webley, P. A. Formation and Photocatalytic Properties of Bismuth Ferrite Submicrocrystals with Tunable Morphologies. *New J. Chem.* **2011**, *35* (4), 937–941.

(42) Wu, T.; Liu, L.; Pi, M.; Zhang, D.; Chen, S. Enhanced Magnetic and Photocatalytic Properties of $Bi_2Fe_4O_9$ Semiconductor with Large Exposed (001) Surface. *Appl. Surf. Sci.* **2016**, *377*, 253–261.

(43) Sun, Y.; Xiong, X.; Xia, Z.; Liu, H.; Zhou, Y.; Luo, M.; Wang, C. Study on Visible Light Response and Magnetism of Bismuth Ferrites Synthesized by a Low Temperature Hydrothermal Method. *Ceram. Int.* **2013**, *39* (4), 4651–4656.

Chapter 3.

Conclusions and Future Work

3.1 Conclusions

The goal of this thesis was to study the effects of potassium and sodium cations used during hydrothermal synthesis (HTS) of bismuth iron oxide (BFO) crystals. Before explaining the experiments to investigate these effects, I first discussed what hydrothermal synthesis is, why we wanted to synthesize bismuth iron oxides, and how cations may affect synthesis.

Hydrothermal synthesis is a synthetic method where crystals form in solution in a closed reaction vessel. Because the reaction vessel is sealed, aqueous solutions can be heated to temperatures above boiling point without loss of solvent. Contrary to traditional solid-state syntheses, solution synthesis uses the solvent to mediate transportation and complexation of solutes to allow facile growth of materials that are otherwise difficult to synthesize. Hydrothermal synthesis has been shown to be able to produce complex oxide-containing materials, including BFOs, with good phase selectivity.

The three BFO phases of interest are $BiFeO_3$, $Bi_2Fe_4O_9$, and $Bi_{25}FeO_{40}$. These three phases form crystals with different structures and thus properties. Each has been shown to have semiconductor and catalytic properties, but initial interest in $BiFeO_3$ was due to its promise as a room-temperature magnetoelectric material. The relationship between these three is that traditional syntheses of one often results in the synthesis of the other two as impurities. Thus, the demonstrated ability of hydrothermal synthesis to produce

each phase separately or with each other shows promise for the extension of HTS to other materials. In HTS, it has been discovered that $Bi_{25}FeO_{40}$ forms as a stable crystal at room-temperature, but is replaced by $BiFeO_3$ or $Bi_2Fe_4O_9$ upon heat treatment. The resultant $BiFeO_3$ and $Bi_2Fe_4O_9$ crystals can have a variety of shapes and sizes, depending on the parameters and additives in the synthesis.

Ions contribute to ionic strength which has a known influence on the activity of species in solution. Spectator ions contribute to the ionic strength while also not reacting with other materials, making them ideal additives to control ionic strength. However, ions in high concentrations have been shown in a variety of systems to influence syntheses in other ways. For example, they are known to incorporate in some crystal structures as impurities and to adsorb onto growing crystals, affecting kinetics and growth of those crystals. In HTS of BFOs, early papers showed a correlation between the spectator cation on the base and the final crystal structure, but were unable to explain why this relationship existed. Using the recent discovery of the link between intermediate phase $Bi_{25}FeO_{40}$ and final phases $BiFeO_3$ or $Bi_2Fe_4O_9$, we sought to investigate how two common base cations, K^+ and Na^+, affected reaction pathways for formation of BFOs.

We started our investigation by comparing the results of 4 sets of related synthesis conditions (varying the Bi^{3+} and Fe^{3+} concentrations, the OH^- concentration, and a room temperature reaction time). With KOH, one set of conditions led to the formation of phase-pure $BiFeO_3$ while another led to phase-pure $Bi_2Fe_4O_9$. The other two conditions led to mixed phases of $BiFeO_3$ and $Bi_2Fe_4O_9$. With NaOH, all of the sets of tested conditions led to phase-pure $Bi_2Fe_4O_9$.

We wanted to understand whether the final phase differences were due to the cations changing the intermediate phases formed before furnace reaction. It was previously discovered that crystalline $Bi_{25}FeO_{40}$ phase nucleates out of an otherwise amorphous intermediate at room temperature given a sufficient amount of time[1,2]. The presence of $Bi_{25}FeO_{40}$ phase was correlated to preferential formation of $BiFeO_3$ when KOH was the base. Building on these results, we found that $Bi_{25}FeO_{40}$ can form regardless of the base used, indicating spectator K^+ and Na^+ do not affect the formation of this crystalline intermediate. However, even with the formation of $Bi_{25}FeO_{40}$, only $Bi_2Fe_4O_9$ formed in NaOH. We concluded that, because it forms in either base, $Bi_{25}FeO_{40}$ may not actually cause a final phase preference. Subsequently, we hypothesized that the amorphous component of the intermediate was affected by the cations and that this component was responsible for the final phase preference.

We developed a two-step "drip-resuspension" method that would allow us to compare the individual effects of different spectator ions on the intermediate. Our hypothesis was that if the amorphous intermediate was responsible for the final phase preference, then the cations cause different intermediates to form. Then, the special intermediate should cause a preferred phase to nucleate during furnace treatment regardless of the base in which it is heated. This method consisted of precipitating out both the amorphous and crystalline intermediate in one base, washing off soluble ions including the base cation, and then furnace reacting it in another base. Our results suggested that the cations themselves cause the final phase preference – the final phase corresponded to whichever cation was present during the furnace reaction (K^+ for $BiFeO_3$ and Na^+ for $Bi_2Fe_4O_9$). We were not able to directly verify if the amorphous

intermediate changed due to the base that it was precipitated in but showed that the cation present during the precipitation seemingly had no effect on the final phase. We noted that $Bi_{25}FeO_{40}$ was also present as a final phase when NaOH was the final base, but not when KOH was the final base. We conjectured that washing off spectator NO_3^- anions during drip-resuspension destabilized free Bi^{3+} and Fe^{3+} ions or complexes in the solution, providing a driving force to form $Bi_{25}FeO_{40}$ from leftover Bi^{3+} and Fe^{3+} after formation of $Bi_2Fe_4O_9$. We conducted thought experiments comparing likely scenarios for $Bi_{25}FeO_{40}$ formation with our conjecture in mind. The only scenario that matched our observations was if NO_3^- is an ion stabilizer and $Bi_{25}FeO_{40}$ dissolves during heat treatment and then reprecipitates from leftover ions. These thought experiments provided reasoning that suggests that $Bi_2Fe_4O_9$ does not form through the same reaction pathway as $BiFeO_3$.

Finally, we wanted to understand how crystal morphology was affected by spectator ions. We noticed a small loss of facet definition for $BiFeO_3$ crystals prepared by drip-resuspension versus those prepared without. In experiments without drip-resuspension, $Bi_2Fe_4O_9$ took the form of thin, rectangular plates. Comparatively, $Bi_2Fe_4O_9$ crystals in the $Bi_2Fe_4O_9$ and $Bi_{25}FeO_{40}$ mixture produced by drip-resuspension suffered from severe degradation in crystal definition to the point that they were visually indistinguishable from aggregated $Bi_{25}FeO_{40}$.

Given our results, we hypothesized a crystal stabilization role for anions and a phase control role for cations. We were not able to conclude a mechanism for how these ions bring about the observed changes. Analyzing the mechanisms will require the use of

more sophisticated techniques such as cryogenic and liquid-phase TEM and is outside of the scope of this work.

Up to this work, others had also identified the role spectator cations play in phase determination of the product[3,4], but no one had specifically pinpointed the relative importance of the cation to be during the furnace treatment and not before. Observing the effects of spectator ions on the formation of the intermediate and then understanding how the intermediate transforms in the presence of spectator ions had not been reported before. The drip-resuspension process described here can be used with little modification to explore the effects of other spectator ions in the HTS of BFOs.

3.2 Future Work and Ideas to Guide It

Future work would extend the applicability of the drip-resuspension process to anions in particular and other spectator ions in general. In conjunction with work to identify other intermediate compounds, this method could be used to more precisely control when and what spectator ions are put into solution, promoting better phase and morphological control. More precise control would allow flexible design of complex experiments intended to understand reaction pathways and mechanisms. For example, understanding would be made possible for whether mixing spectator ions is simply additive of each individual species' effects or how low and high concentrations of spectator ions alter the formation of intermediate compounds differently. Finally, demonstrating the successful use of this method to elucidate the function of even the most commonly included spectator ions (i.e. Li^+, Na^+, K^+, NO_3^-, Cl^-) would improve the ability of HTS to produce tailored BFO crystals. In turn, these results could be used to

hydrothermally synthesize other materials that present a competition between phases that are similar in energy and stabilities.

The following are some thoughts and ideas for specific experiments to conduct in the future:

Morphology control – anionic link

Some papers in the literature suggest that spectator anions have an effect on crystal morphology.[5–8] However, before this thesis work, there had been no reliable methods to isolate and study the effects of specific spectator ions. Thus, studies that produce uncommon crystal shapes have been unconvincing in their determination of what causes the shapes, or at the very least, that anions specifically cause morphology change.

Usually, any HTS of BFOs requires the use of high concentrations of base. Because most bases used are OH^- bases, a correspondingly large amount of counter-ion is also present in solution. Using this requirement as an advantage, one can add extra salt of the same cation at low concentrations to effectively determine the effects of low concentrations of spectator anions.

For example, if I use 9 M KOH, I can add 1 M KNO_3 to test the effects of NO_3^-. The addition of salt results in a minor increase in the spectator cation (11% increase of K^+ concentration, in this case), but would allow one to perform systematic studies comparing the effects of different anions at low concentrations.

3.3 References

(1) Lopes, A. M. L.; Araújo, J. P.; Ferdov, S. Room Temperature Synthesis of $Bi_{25}FeO_{39}$ and Hydrothermal Kinetic Relations between Sillenite- and Distorted Perovskite-Type Bismuth Ferrites. *Dalt. Trans.* **2014**, *43* (48), 18010–18016.

(2) Goldman, A. R.; Fredricks, J. L.; Estroff, L. A. Exploring Reaction Pathways in the Hydrothermal Growth of Phase-Pure Bismuth Ferrites. *J. Cryst. Growth* **2017**, *468* (September 2016), 104–109.

(3) Wang, Y.; Xu, G.; Yang, L.; Ren, Z.; Wei, X.; Weng, W.; Du, P.; Shen, G.; Han, G. Alkali Metal Ions-Assisted Controllable Synthesis of Bismuth Ferrites by a Hydrothermal Method. *J. Am. Ceram. Soc.* **2007**, *90* (11), 3673–3675.

(4) Tsai, C. J.; Yang, C. Y.; Liao, Y. C.; Chueh, Y. L. Hydrothermally Grown Bismuth Ferrites: Controllable Phases and Morphologies in a Mixed KOH/NaOH Mineralizer. *J. Mater. Chem.* **2012**, *22* (34), 17432–17436.

(5) Wang, Y.; Xu, G.; Ren, Z.; Wei, X.; Weng, W.; Du, P.; Shen, G.; Han, G. Mineralizer-Assisted Hydrothermal Synthesis and Characterization of $BiFeO_3$ Nanoparticles. *J. Am. Ceram. Soc.* **2007**, *90* (8), 2615–2617.

(6) Zhu, X.; Hang, Q.; Xing, Z.; Yang, Y.; Zhu, J.; Liu, Z.; Ming, N.; Zhou, P.; Song, Y.; Li, Z.; et al. Microwave Hydrothermal Synthesis, Structural Characterization, and Visible-Light Photocatalytic Activities of Single-Crystalline Bismuth Ferric Nanocrystals. *J. Am. Ceram. Soc.* **2011**, *94* (8), 2688–2693.

(7) Liu, Y.; Zuo, R. Morphology and Optical Absorption of $Bi_2Fe_4O_9$ Crystals via Mineralizer-Assisted Hydrothermal Synthesis. *Particuology* **2013**, *11* (5), 581–587.

(8) Zhou, M.; Li, W.; Du, Y.; Kong, D.; Wang, Z.; Meng, Y.; Sun, X.; Yan, T.; Kong, D.; You, J. Hydrothermal Synthesis of Bismuth Ferrite Fenton-like Catalysts and Their Properties. *J. Nanoparticle Res.* **2016**, *18* (11), 346 (1-15).

APPENDIX

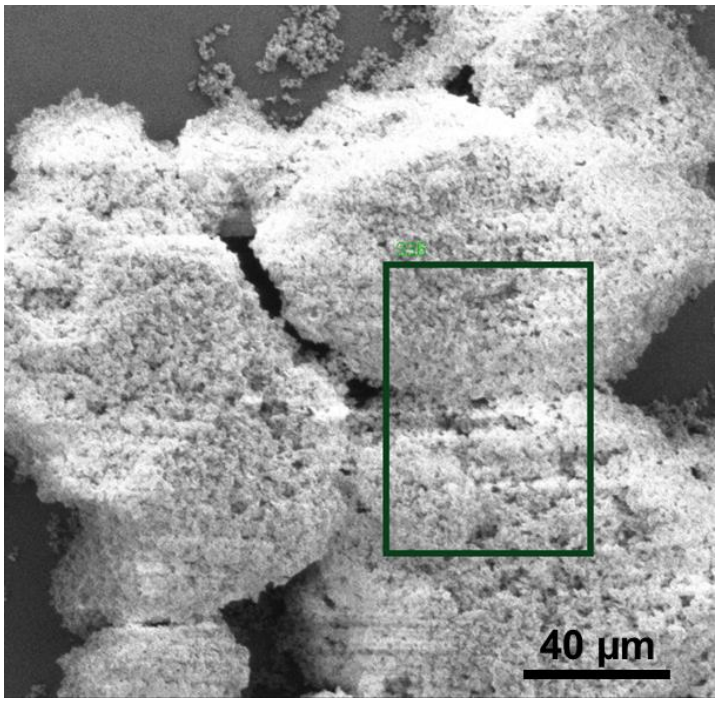

Figure S1: EDX of $Bi_{25}FeO_{40}$

The green box represents a representative area of the sample of $Bi_{25}FeO_{40}$ + $Bi_2Fe_4O_9$ that underwent EDX analysis. The table below contains the raw data for the analysis. Headings from left to right: **Element, Atomic number, Normalized Mass ± Absolute Error** (of measurement)**, Atomic Composition**.

Element	Atomic. No.	Norm. Mass ± Abs. Error (1 σ) [%]	Atom. Comp. [%]
Oxygen	8	9.88 ± 1.52	53.18
Bismuth	83	81.55 ± 3.89	33.60
Iron	26	8.57 ± 1.56	13.22
	SUM	100.00 (± error)	100.00

S2: Ionic strength calculation

Ionic strength, *I*, is defined as:

$$I = \frac{1}{2}\sum_i c_i z_i^2$$

where *c* is the concentration of species *i*, and *z* is the charge on the species *i*.

The materials used in an arbitrary synthesis under 100/9/48 conditions are as follows: 9 M KOH, 100 mM $Bi(NO_3)_3$, 100 mM $Fe(NO_3)_3$

The ionic strength for a solution contain the above is:

$$I = \frac{1}{2}(9M\ K^+ \times (+1)^2 + 9M\ OH^- \times (-1)^2 + 0.1M\ Bi^{3+} \times (+3)^2 + 0.1M\ Fe^{3+} \times (+3)^2 + 0.6M\ NO_3^- \times (-1)^2)$$

$$I = \tfrac{1}{2}(9M + 9M + 0.9M + 0.9M + 0.6M)$$

$$I = \frac{1}{2}(20.4\ M) = 10.2\ M$$

Repeating the same calculations for the above, but without NO_3^- yields:

$$I = 9.9\ M$$

Then, the change in ionic strength due to washing off NO_3^- is:

$$I = \frac{10.2M - 9.9M}{10.2M} \times 100\% = 2.9\%$$